Award Number: W81XWH-10-1-0843

TITLE: In Vivo PET Imaging of Myelin Damage and Repair in the Spinal Cord

PRINCIPAL INVESTIGATOR: Robert Miller

CONTRACTING ORGANIZATION: Case Western Reserve University
Cleveland, OH 44106

REPORT DATE: October 2011

TYPE OF REPORT: Annual

PREPARED FOR: U.S. Army Medical Research and Materiel Command
Fort Detrick, Maryland 21702-5012

REPORT DOCUMENTATION PAGE

Form Approved
OMB No. 0704-0188

1. REPORT DATE *(DD-MM-YYYY)*	**2. REPORT TYPE**	**3. DATES COVERED** *(From - To)*
01-10-2011	Annual	30 Sep 2010 - 29 Sep 2011

4. TITLE AND SUBTITLE
In Vivo PET Imaging of Myelin Damage and Repair in the Spinal Cord

5a. CONTRACT NUMBER

5b. GRANT NUMBER
W81XWH-10-1-0843

5c. PROGRAM ELEMENT NUMBER

6. AUTHOR(S)
Robert Miller

E-Mail: rhm3@case.edu

5d. PROJECT NUMBER

5e. TASK NUMBER

5f. WORK UNIT NUMBER

7. PERFORMING ORGANIZATION NAME(S) AND ADDRESS(ES)
Case Western Reserve University
Cleveland, OH 44106

8. PERFORMING ORGANIZATION REPORT NUMBER

9. SPONSORING / MONITORING AGENCY NAME(S) AND ADDRESS(ES)
U.S. Army Medical Research and Materiel Command
Fort Detrick, Maryland 21702-5012

10. SPONSOR/MONITOR'S ACRONYM(S)

11. SPONSOR/MONITOR'S REPORT NUMBER(S)

12. DISTRIBUTION / AVAILABILITY STATEMENT
Approved for Public Release; Distribution Unlimited

13. SUPPLEMENTARY NOTES

14. ABSTRACT

During the first funding cycle, we have worked closely with Dr Wang to develop a series of animal models to assess the efficacy of the imaging compounds that he has developed to detect demyelination and remyelination in the intact brain and spinal cord. We have also begun to test the ability of the imaging probes to assay remyelination in response to potential therapeutic treatments. The key research accomplishments are highlighted below:

1. Design, synthesis and evaluation of coumarin-based molecular probes for imaging of myelination. (Wang et al, J. Med. Chem. 2011)
2. Longitudinal imaging of myelination using a near infra-red probe. (Wang et al, J. Neuroscience 2011)
3. Longitudinal [11C]CIC-PET Imaging in the spinal cord of a rat model of focal demyelination.

15. SUBJECT TERMS
Positron emission tomography, imaging, myelination, molecular probes, multiple sclerosis

16. SECURITY CLASSIFICATION OF:			**17. LIMITATION OF ABSTRACT**	**18. NUMBER OF PAGES**	**19a. NAME OF RESPONSIBLE PERSON**
a. REPORT	**b. ABSTRACT**	**c. THIS PAGE**			USAMRMC
U	U	U	UU	35	**19b. TELEPHONE NUMBER** *(include area code)*

Table of Contents

Page

Introduction

Myelination is critical for the functioning of the adult vertebrate nervous system development (Sherman and Brophy, 2005). Myelin sheaths provide a unique structure in the nervous system that promotes rapid and efficient conduction of impulses along axons as well as protecting axons from damage (Hildebrand et al., 1993). Abnormalities or changes in myelin occur in many acquired or inherited neurodegenerative diseases including multiple sclerosis (MS) and various leukodystrophies (Hauw et al., 1992) where they result in functional deficits. Multiple sclerosis, which affects an estimated 350,000 people in the US and 2 million people worldwide, is the most commonly acquired demyelinating disease in humans (Compston and Coles, 2002). Both acquired and inherited myelin disorders share a poor prognosis often leading to major disability by young adulthood.

Recently, a disproportionate number of Gulf War veterans have reported neurological problems years after their service. Mounting evidence suggested that a "service-connected" link might exist in the diagnosis of MS among US veterans (Wallin et al, 2004). The significant increase of MS in US veterans has become a key area of congressionally-directed research programs, yet early diagnosis of MS and tracking of disease progression remains a difficult challenge. The majority of the current treatment options for MS are directed at regulation of the pathogenic activities of the patient's immune system, rather than at repair of myelin in the CNS. However, new therapeutic agents are being developed aimed at myelin repair. The effective monitoring of myelin changes is difficult and assessing the degree of demyelination subjective. This is due in large part to the fact that the use of magnetic resonance imaging (MRI) as a primary outcome measure of disease activity has been shown to be dissociated from the clinical attack rate in disease-modifying therapies (Molyneux et al., 2001). In MRI, any change in signal intensity reflects a change in tissue water content, which is a non-specific measure of the overall changes in macroscopic tissue injury that might range from edema and inflammation to demyelination and axonal loss (Filippi et al., 2005). To better assist the military in battling neurological disorders among its veterans, and developing new effective therapies for MS, molecular imaging tools must be developed that can be used to directly quantify myelin changes *in vivo*.

Over the past decade, the two PIs of this application have independently devoted their efforts to MS research in myelin imaging and myelin repair therapy, respectively. On one side, Dr. Wang and his team have developed a new myelin-imaging technique based on positron emission tomography (PET) for *in vivo* studies of the pathogenesis and progression of MS. On the other side, Dr. Miller and his team have focused on understanding oligodendrocytes (the myelinating cells of the CNS) and myelin biology and developed several new therapeutic agents that appear to promote remyelination, an activity that is likely critical for sustained functional recovery. The results from the last year are highlighted below and these form the basis for the synergistic collaboration to develop an imaging guided drug discovery approach to myelin repair in MS.

Body

With the continuation of this Synergistic Idea Award from the Department of Defense, we will further optimize the newly developed myelin-imaging techniques and use them to evaluate the efficacy of novel therapeutic agents in different animal models of MS. These studies will allow us to identify the best candidate(s) of myelin probes that are uniquely suited for future clinical trials. *We hypothesize that myelin repair can be achieved by therapeutic agents that are aimed at promotion of remyelination. Further, we specifically hypothesize that the efficacy of remyelinating agents can be quantified in vivo through the use of imaging probes at various*

levels of myelination such that the regional distribution and concentration of probes will be consistent with the myelin neuropathology present. Our approach will be to continue the further develop of myelin-imaging agents that can longitudinally monitor myelin changes in different animal models of demyelination. Next, we will use PET imaging to evaluate the *in vivo* myelin repair properties of therapeutic agents. We will then validate the *in vivo* studies by correlation with postmortem histology studies. Completion of this project will allow us to identify the lead candidate for Phase I clinical trial that can be initiated immediately following completion of this project.

During the first funding cycle Dr. Wang has further optimized the imaging techniques by developing some additional myelin imaging agents. Dr. Miller has used a number of different animal models to examine the efficacy of those imaging probes to identify areas of demyelination and remyelination in the adult vertebrate CNS. The results obtained through longitudinal imaging with the novel probes were correlated with histological outcomes. Finally, studies aimed at assessing the capability of the newly developed probes to illuminate the efficacy of remyelinating directed therapies have been initiated. To accomplish these outcomes we have utilized a range of approaches that combine novel and established protocols in the Miller laboratory.

Specific Aim 1: Preparation of animal models of normal and dysmyelinated phenotype.

Major Task 1: Obtain eight-week old C57BL/6 mice and C3Fe.SWV-Mbpshi/J shiverer mice for optimization of myelin imaging agents through tissue staining.

Rationale for the selection of the model systems: The overall goal of the proposed studies is to develop probes that will allow for the longitudinal characterization of the level of myelination in defined regions of the adult vertebrate CNS. To screen potential probes generated by the Wang laboratory we have utilized approaches that allow for good tissue preservation as well as the retention of antigenicity or the capacity of the probes to bind in a specific manner.

A. Materials and Methods:

In this section, the preparation of animal models, tissue processing and staining, immunohistochemistry, and statistical methods are described. The chemical and synthetic procedures are described in the progress report of the PI, Dr. Wang.

A.1 All animal experiments were performed in accordance with the guidelines approved by the Institutional Animal Care and Use Committee of Case Western Reserve University (Protocol 2006-0176). Animals were housed in the ARC and brought into the surgery suite of the miller laboratory for all treatments. Imaging probes were delivered to the animals through a tail vein injection using an animal restraining system that results in minimal stress. Eight-week old C57BL/6 mice and C3Fe.SWV-Mbpshi/J shiverer mice were obtained from The Jackson Laboratory, Bar Harbor, ME and allowed to adjust to their surroundings for 3-4 days prior to injections.

A.2 Euthanasia and perfusion protocol. To obtain tissue that was well preserved anatomically as well as biochemically, a rapid fixation protocol was utilized. Mice were terminally anesthetized with isoflurane and just prior to death the chest cavity was opened and tubing inserted into the ascending aorta. Using a rotary pump pressured system the animals were flushed with PBS (released through hepatic vein) to removed blood and serum proteins and then fixed with at least 10X volumes of 4% paraformaldehyde in PBS. Following fixation, the brains,

spinal cords and sciatic nerves were removed and incubated for 24 hours in fresh 4% paraformaldehyde at 4°C.

A.3 Tissue processing. To obtain sections that allowed for the effective localization of the binding of the probes, frozen sections were generated from selected regions of the nervous system. To prepare frozen sections, brain and sciatic nerve tissue were rinsed in PBS. After treatment with 4% PFA overnight, the tissues were incubated in 30% sucrose until submerged. For preparation of fresh frozen sections, the cryoprotected tissues were first frozen in OCT on dry ice before axial sectioning (20μm) with a cryostat at -20°C. Tissue sections from the midline of the brain containing the whole corpus callosum were selected for staining. Stained sections were covered with fluorescence mounting medium (Vectashield, Vector Laboratories, Burlingame, CA) and stored at 4°C for future analysis.

A.4 Chemical staining. Fresh frozen sections with 20μm in thickness were incubated in 0.1% Triton-100 in 1xPBS for 10 minutes and then incubated in a solution of compounds (100μM) in 10% DMSO/H_2O for 30 minutes at room temperature. The fresh frozen sections were then washed three times for 5 minutes each with PBS before cover slipping with fluorescence mounting medium. Images of the stained mouse brain sections were acquired on a Leica DMI5000 inverted microscope (BP470/40 nm filter) and the images collected with a cooled CCD.

A.5 Immunohistochemistry. Fresh frozen sections were rinsed in 3% normal goat serum in 0.1% TritonX-100/PBS three times for 5 minutes each and washed with PBS three times for 5 minutes each. The sections were then immunostained overnight at 4°C with purified mouse antibody monoclonal (Covance, Inc., Princeton, NJ) 1:500 dilution in 3% normal goat serum in 1xPBS. Sections were incubated for 1 hour at room temperature in Cy3 AffiniPure Goat Anti-Mouse IgG (H+L) (Jackson ImmunoResearch Laboratores, Inc., West Grove, PA) and rinsed in PBS three times for 5 minutes each. Images of the stained mouse brain sections were acquired on a Leica DMI5000 inverted microscope (BP 645/75 filter).

A.6 Black-Gold II staining. To independently identify regions of the CNS that expressed high levels of compact myelin, a Black-Gold labeling approach was used. Unlike antibodies to myelin proteins such as Myelin Basic Protein (MBP) that detect myelin proteins regardless of the level of myelin compaction, Black Gold labeling predominately recognizes compact myelin. A 0.3% solution of Black-Gold II was made by adding 150 mg of Black-Gold II to 50ml of 0.9% NaCl. The solution was fully equilibrated to 60°C in a water bath. Sections mounted on superfrost coated slides (Fisher Scientific) were transferred to the warm Black-Gold II impregnating solution in the water bath and the staining was visually monitored. Images of the stained mouse brain sections were acquired on a Leica DMI5000 inverted microscope under bright field illumination. To confirm that the Black Gold labeling accurately reflected the differential expression of myelin proteins, consecutive sections were labeled with antibodies to MBP and probe. To detect MBP, frozen sections mounted on superfrost slides were labeled using the protocols described in **A5**.

A.7 Detection of probe binding to normal neural tissue *in vivo*. To determine whether the probes were effective at crossing the blood brain barrier and labeling the CNS in living animals, the probes were delivered via intravenous injection and their binding visualized to the brain tissue in frozen sections following fixation. To deliver the probes, under anesthesia, wild-type mice were injected with compounds FCP (40 mg/kg) via the tail vein, and following variable survival times the mice were sacrificed by transcardial perfusion with saline followed by 4% PFA in PBS. Brain tissues were then removed, post-fixed by

immersion in 4% PFA overnight, dehydrated in 30% sucrose solution, cryostat sectioned at 20μm on a microtome and mounted on superfrost slides (Fisher Scientific). For the direct detection, the sections were cover slipped with fluoromount mounting media (Vector Laboratories, Burlingame, CA). Images of the stained mouse brain sections were acquired on a Leica DMI5000 inverted microscope (BP470/40 nm filter). For the immunohistochemical co-staining, the sections were stained with anti-MBP antibody following the procedure described in **A.6**.

A.8 *In vivo* visualization of probe binding to peripheral nerves. To determine whether probes could bind to peripheral nerves, eight-week old C57BL/6 black mice were administered via tail vein injection a dose of 40 mg/kg of FCP using saline as the vehicle. Ten minutes post-injection, the mice were terminally anesthetized with isoflurane. Sciatic nerves in the leg regions were then surgically exposed and imaged using a Leica M216FA dissection fluorescent microscope (LP 590 filter). After imaging, the mice were perfused as described above then the sciatic nerves were again imaged.

A.9 Quantification and statistical analysis. ImageJ software (http://rsb.info.nih.gov/ij/) was used to quantify pixel intensities values. The corpus callosum between the midline and below the apex of the cingulum was defined as ROI. The density of myelin in the corpus callosum of wild-type mice was given the arbitrary value of 100, and the density of myelin in Plp-Akt-DD mice was determined as a percentage of wild-type mice. The data were analyzed using the GraphPad Prism (GraphPad Software, La Jolla, CA) with a non-paired Student's t test.

B. Results: Characterization of the binding properties of different probes and probe selection.

In this report, we have focused specifically on the activities of the Co-PI of this application. The division of labor in this program is that the PI, Dr. Wang, is responsible for the generation of the new probes while Dr. Miller is responsible for the animal model and the histological characterization. To date, Dr. Wang has generated a series of small molecular probes (SMPs) that readily penetrate the blood-brain barrier and selectively bind to myelin with high affinity and specificity (**Figure 1**).

Figure 1

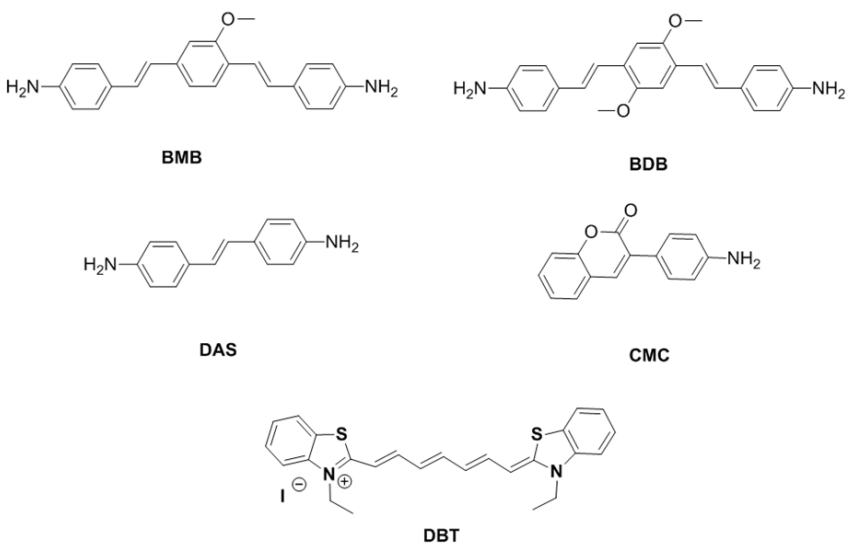

Figure 1. The myelin-imaging agents for *in vivo* imaging studies. BMB, BDB and DAS were precursors of PET imaging radiotracers. DBT was a novel myelin-specific optical imaging probe. BMB: (*E, E*)-1, 4-bis (p-aminostyryl)-2-methoxy-benzene; BDB: (*E, E*)-1, 4-bis (4′-aminostyryl)2,5-dimethoxy-benzene; DAS: 4, 4′-diamino-

trans-stilbene; CMC: 3-(4-aminophenyl)-2Hchromen-2-one; DBT: 3, 3′-Diethylthiatricarbocyanine iodide.

During the course of these studies, Dr. Wang focused on the design and synthesis of a series of coumarin derivatives as myelin-imaging agents and generated 36 coumarin derivatives that were subsequently evaluated through *in vitro* fluorescent tissue staining and *in vivo* fluorescent imaging. These studies allowed us to identify some lead compounds suitable for myelin imaging in clinically relevant settings. The chemical synthesis is described in the report from Dr. Wang.

Compound screening. All of these compounds are fluorescent, which allowed us to examine their myelin-binding properties by fluorescent microscopy. Thus, **1-36** were screened for binding specificity for myelin by histological staining of mouse brain tissue sections. At a concentration of 100 μM of each compound, whole mouse brain tissue sections containing the white matter and gray matter were incubated for 20 minutes at room temperature. The myelin-binding specificity was quantitatively examined by fluorescent intensity in different brain regions. The cellular composition of the brain differs in different regions with respect to the number of oligodendrocytes and the amount of myelin. In gray matter regions such as the cerebral cortex there is a high concentration of neuronal cell bodies and dendrites while in the corpus callosum there is a high concentration of myelinated axons, and few if any neuronal cell bodies. Astrocytes, the third major cell type in the CNS are uniformly distributed between gray and white matter. Based on these data we selected specific areas in which to assay the differential binding of different probes. We hypothesized that probes of interest, namely those that showed selectively for compact myelin would preferentially bind to white matter over gray matter.

Based on the fluorescent tissue staining and fluorescent intensity in the pre-defined region of the corpus callosum, compounds **1-36** were divided into three groups: (1) compounds including **1-17** which showed no binding to compact myelin; (2) **18-26** which showed moderate binding to myelin; and (3) **27-36** which showed high binding. We then further calculated the fluorescence intensity ratio between the white matter and gray matter using pre-defined regions of interest (ROI) as shown in **Figure 2A**.

(A)

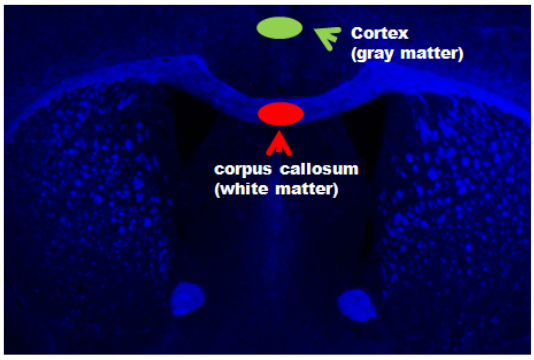

(B)

Compounds NO.	Structure	Fluorescence Intensity Ratio (white matter/gray matter)
27	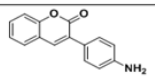	1.39 ±0.01
28	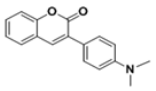	1.34±0.10
29	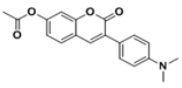	1.35±0.06
30	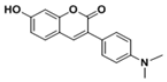	1.25±0.08
31	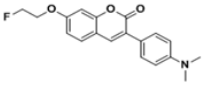	1.52±0.20
32	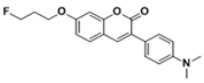	1.54±0.07
33	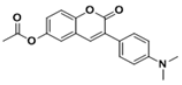	1.53±0.14
34	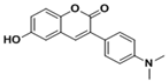	1.48±0.20
35	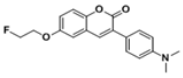	1.33±0.08
36	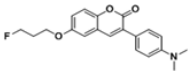	1.38±0.04

(C)

Compounds	Structure	Electron Density on the Nitrogen	Fluorescence Intensity Ratio (white matter/gray matter)
31	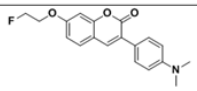	0.326158	1.52±0.20
35	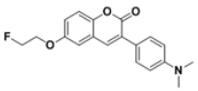	0.448229	1.33±0.08
32	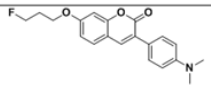	0.326154	1.54±0.07
36	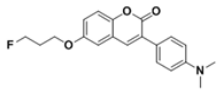	0.448231	1.38±0.04

Figure 2. (A) Regions of interest (ROI) used for quantification of fluorescent intensity and calculation of binding ratios between the white matter and gray matter. (B) The chemical properties and fluorescence intensity analysis. Log P and molecular weight values were calculated by ChemBioOffice 2010, fluorescence intensity ratios were measured by Image J. Statistical analysis was performed with GraphPad Prism 5, La Jolla, CA (average±SD, n=3). (C) Comparison of the electron density of nitrogen and fluorescence intensity ratios of **31, 32, 35** and **36;** less electron density of the nitrogen is preferred to enhance the white/gray matter ratio. Therefore, **32** was an ideal probe for further studies. The electron density of nitrogen is calculated using the Hückel method by ChemBioOffice 2010. Based on these considerations and the differential binding between gray and white matter probe 32 was selected for further study. Probe 32 was termed FPC.

Detection of the binding of probe 32 to CNS and PNS myelin. To assess in more detail the binding properties of probe **32** to myelin in the brain, coronal frozen section through forebrain including the corpus callosum as well as sections through the cerebellum were incubated directly with the probe. Localization of myelin was independently demonstrated through binding of black gold or anti-MBP antibodies. Binding to peripheral nerve was assessed in the sciatic nerve and compared to black gold labeling. At 100μM concentration, **32** selectively labeled corpus callosum (**Figure 3A**) and cerebellum (**Figure 3C**) in the CNS as well as the sciatic nerves in the PNS (**Figure 3E**). The **32** staining patterns were found to be virtually identical to the patterns

observed in immunohistochemical staining for MBP (**Figure 3B, D**) or Black-Gold II staining (**Figure 3F**).

Figure 3

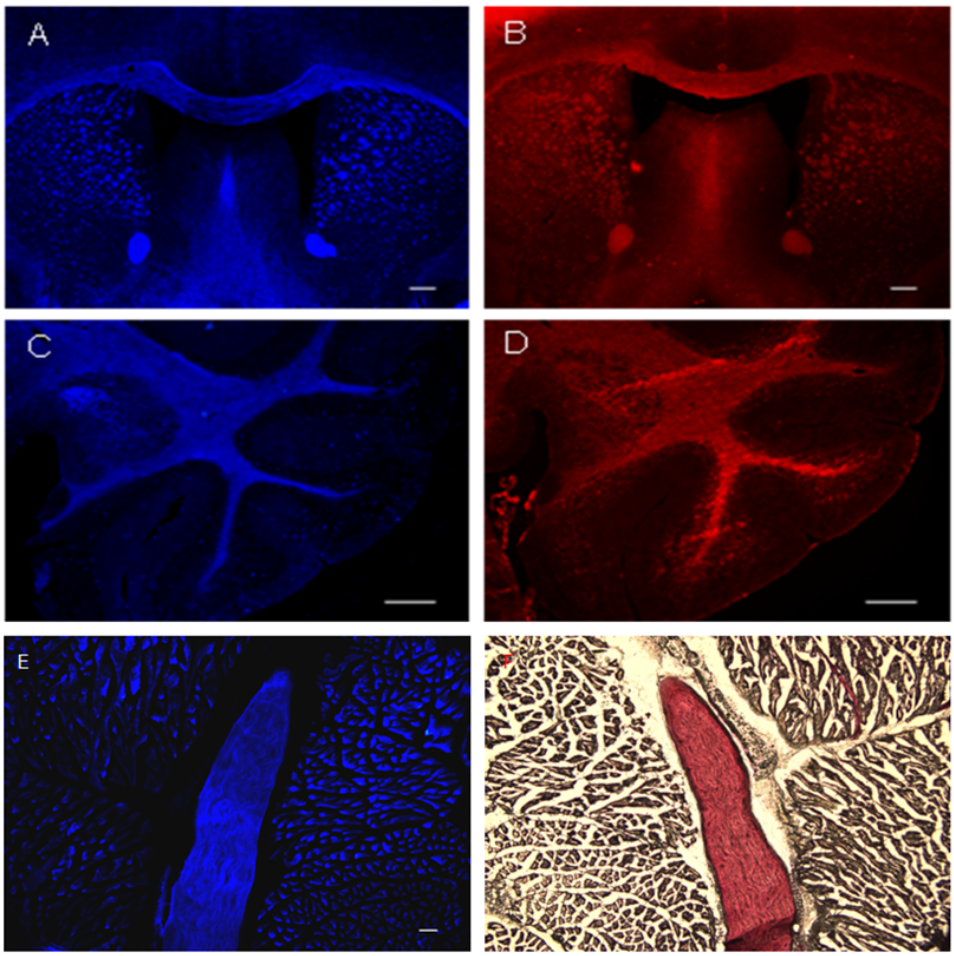

Figure 3. *In vitro* 32 staining of the whole mouse brain (A), cerebellum (C), and sciatic nerve (E). For comparison, the same sections were used for MBP staining of the whole mouse brain (B), cerebellum (D) and for Black-gold II staining of sciatic nerves (F). Scale bar: A, B=500 µm, C, D=300 µm, E, F=100 µm.

These studies provide strong evidence that probe 32 binds selectively to white matter, but do not unequivocally demonstrate this is a result of binding to compact myelin. To directly address this question the studies were repeated using identically treated sections from Shiverer mouse. The Shiverer mouse is a spontaneous mutant that essentially lacks MBP and as a result fails to generate compact myelin sheaths in the CNS. The animals have a limited life span and die during the 2nd - 3rd month of life. All other elements of white matter are present in the Shiverer and thus it provides a direct test for the specificity of probe 32 for myelin.

Labeling of sections of Shiverer brains revealed a dramatic reduction in the level of probe 32 binding compared to control animals (**Figure 4**). Quantitative analysis indicated that the fluorescent intensity is proportional to the level of myelination present in wild-type (**Figures 4A, 4C**) and shiverer mouse (**Figures 4B, 4D**) brains. For example, the fluorescent intensity of MBP antibody binding in shiverer mouse brains was only 14% of that detected in the wild-type control brains **Figures 4E and 4**. Consistent with this data, **32** staining also exhibited a similar fluorescent intensity difference, which was proportional to the level of myelination. In the shiverer mouse brains, the fluorescent intensity of **32** was 12% of that detected in the wild-type mouse brains suggesting that they were binding to similar epitopes.

Figure 4

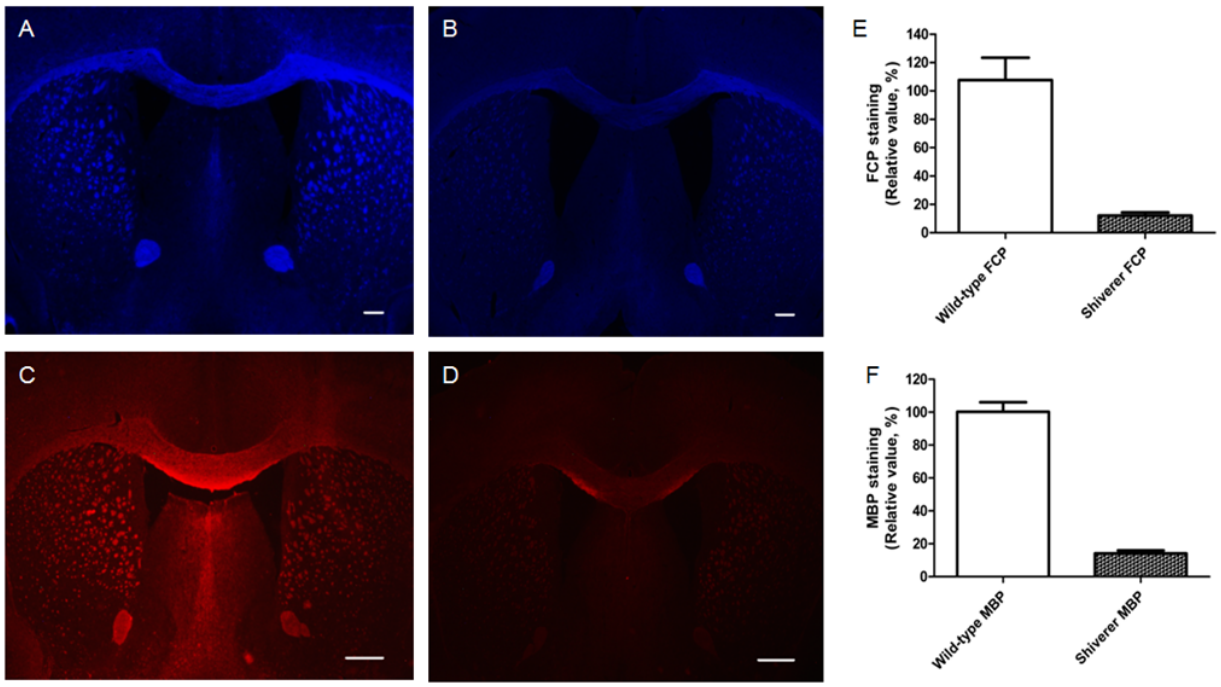

Figure 4. Comparison of **32** staining of the wild-type mouse brain (A) and myelin-deficient shiverer mouse brain (B). Staining with anti-MBP of the same brain sections (C, wild-type; D, shiverer) was also conducted for comparison. Fluorescent intensities in the same corpus callosum region following MBP staining and **32** staining were quantified. The data were analyzed using a GraphPad Prism. (E) P=0.0005, n=3, Unpaired t-test; (F) P<0.0001, n=3, Unpaired t-test. Scale bar: A, B=300 μm, C, D=500 μm.

Probe 32 selectively binds to myelinated regions of the CNS in vivo. To assess whether probe 32 had the properties required for successful longitudinal visualization of myelin in the living animal, the probe was delivered via intravenous injection and the animals subsequently sacrificed, the brains section and probe binding assessed. A dose of **32** (40 mg/kg) was administered to wild-type mice via tail vein injection. One hour post injection, the mouse brains were perfused with saline followed by 4% paraformaldehyde (PFA) and removed. Following fixation the brains were dissected and frozen sections prepared. The fresh frozen brains were then sectioned. Fluorescent staining of myelinated regions such as the cerebellum were then directly examined under a fluorescent microscope. As shown in **Figure 5**, **32** readily entered the mouse brain and selectively labeled heavily myelinated CNS regions in situ.

The nature of **32** binding to myelin was revealed by comparison of **32** staining with immunohistochemical staining for MBP in the cerebellum, caudate putamen, and the temporal cortex regions (**Figure 5**). In the cerebellum, **32** staining was largely confined to deep white matter tracts that contain the majority of myelinated axons whereas MBP staining was also observed in the granule cell layer where there are scattered oligodendrocytes and limited myelin

sheaths. Likewise, in the caudate putamen, **32** selectively stained myelin fibers while MBP also stained oligodendrocyte cell soma and processes. In the temporal cortex, no chemical staining was observed whereas MBP staining revealed the presence of individual myelinated fibers. Strong probe binding was observed in subcortical white matter and corpus callosum. These studies suggest that **32** selectively binds to compact myelin.

Figure 5

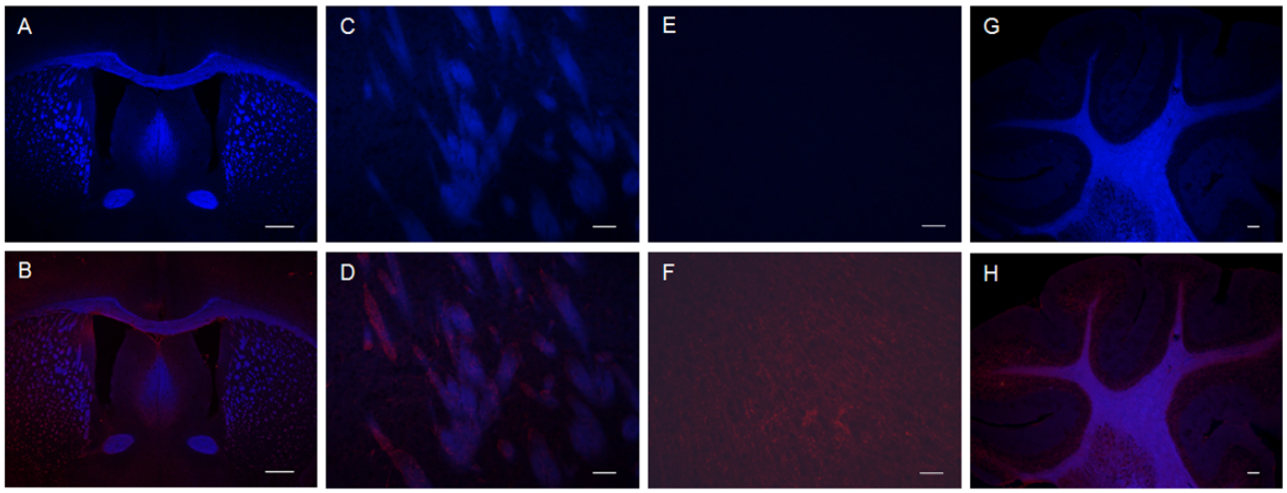

Figure 5. *In situ* **32** chemical staining of the brain (A), striatum (C), fibers in cortex (E) and cerebellum (G), **32** didn't show binding with small fibers in the cortex. Then the stained sections were double-stained with Anti-MBP, and the merged images show the brain (B), striatum (D), fibers in cortex (F) and cerebellum (H). The lack of staining with anti-MBP on the brain, striatum and cerebellum indicated that **32** can bind MBP on the big bundle of myelin sheaths. Scale bar: A, B=500 μm, C, D=50 μm, E, F, G, H=100 μm.

32 Stains PNS Nerves *In Vivo*

To examine the ability of **32** to visualize PNS nerves *in vivo*, **32** (40mg/kg) was administered to wild-type mice via tail vein injection. As shown in **Figure 6**, 10 minutes post injection, bright fluorescence was observed in the sciatic nerves exposed under anesthesia. The fluorescence intensities of the nerves were significantly higher than that detected in the surrounding bones or muscles. Thus, **32** could be used intra-operatively to visualize delicate nerves that are prone to damage during surgical procedures in the operating room. These studies indicated that **32** allowed selective visualization of myelinated nerves *in vivo*.

Figure 6

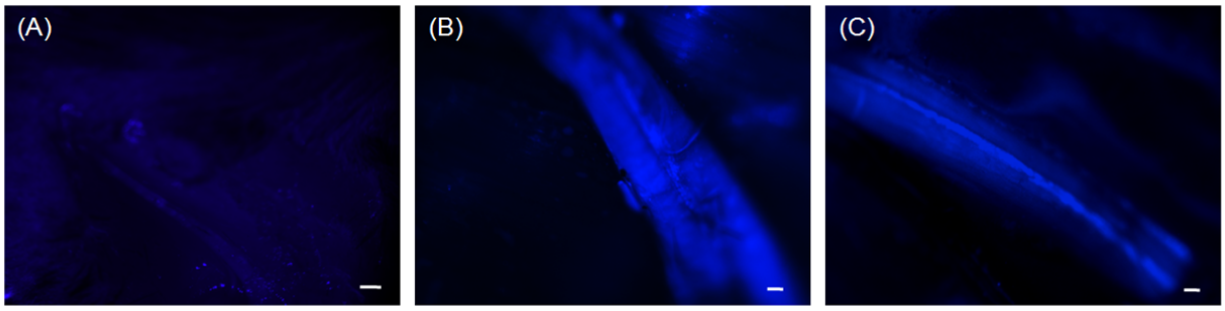

Figure 6. *In vivo* visualization of myelinated nerves following injection of **32** in mice. Image A shows the exposure of sciatic nerves in a mouse under anesthesia at 10 minutes post injection of saline. No fluorescence was observed in sciatic nerves under a dissection fluorescent microscope. At 10 minutes post injection of 40 mg/kg of **32**, strong fluorescence from **32** was observed in the sciatic nerve (B), which also showed better contrast between the sciatic nerve and surrounding tissues. This remained unchanged after perfusion (C) suggesting that **32** fluorescence was in nerves and not blood vessels. Scale bar: A=1 mm. B, C=0.1 mm.

C. Discussion:

The ability to use imaging agents to assess the state of disease in MS in a non-invasive longitudinal manner is critically important. Such data can provide insights into the rate of disease progression and the response to therapies. Multiple sclerosis is a demyelinating disease and to effect long term functional recovery will likely require the capability to stimulate remyelination in the CNS. Currently there are no remyelinating therapies on the market although we, and others, are identifying new targets and developing CNS oriented treatments. The capability to visualize myelin in the intact CNS in a quantifiable manner is the goal of the project and the development of probes such as 32 that cross the blood brain barrier and selectively bind to myelinated regions of the CNS is a major advance. While Dr. Wang continues to refine the chemical nature of the probes to improve specificity and signal to noise ratios Dr. Miller will continue to develop new animal models and therapeutics to test the efficacy of the probes. A critical next step is to determine whether such probes can be effectively labeled for use with detection systems other than fluorescence.

A foremost application of **32** may be in PET imaging of demyelination. In our previous studies, we identified some lead compounds that readily entered the brain and selectively localized in the myelinated regions. These findings provide proof-of-the-concept that small-molecule myelin-imaging probes can be developed via direct binding to myelin membranes. However, all of these imaging probes are radiolabelled with C-11. Due to short half-life (20 min), C-11-labelled probes can only be synthesized on site using a dedicated cyclotron and, therefore, are not suitable for remote distribution. Since most of clinical facilities do not have on site cyclotron, use of C-11-labelled imaging agents is limited. In order to enhance the potential of their clinical applications, myelin-imaging agents have to be radiolabelled with fluorine-18, a positron-emitting radionuclide with a half-life of 110 minutes. F-18-Labelled agents are suitable for regional distribution and thus can be used by PET facilities without an on-site cyclotron. Thus, in

future studies, we plan to thoroughly evaluate F-18-labelled **32** for PET studies in a way similar to widely used 2-fluorodeoxyglucose (FDG). Once developed, it can be commercially distributed across the country for routine clinical studies as is currently done with FDG.

Major Task 2. Preparation and use of Plp-Akt-DD transgenic mice for validation of myelin imaging agents through longitudinal optical imaging studies.

Rationale: The previous studies with the shiverer mutant animals suggest reductions in endogenous compact myelin such as seen in shiverer mice are clearly detectable using the recently developed probes. In this task we asked the question whether the probes could detect increased myelin in the CNS of intact animals. The molecular mechanisms that regulate oligodendrocytes development, myelination and remyelination are relatively poorly understood. Recent studies, however, have begun to identify signaling pathways within oligodendrocytes and their progenitors that modulate critical aspects of their behavior. Work by Dr. Wendy Macklin and colleagues showed that increasing the activity of the protein kinase AKT specifically within cell of the oligodendrocyte lineage resulted in a massive over-production of myelin during development. In fact these animals appear unable to stop generating myelin sheaths and the myelin is much thicker than controls. This imbalance in the axon/myelin ratio (G ratio) is ultimately detrimental and the animals die during the first year of life. Regardless of the biology of the animals they represent an ideal model in which to determine whether the probes developed by Dr. Wang can detect abnormally high levels of myelin in the CNS. To this end we acquired these animals and undertook a comparative study to define probe binding between shiverer, wild type and AKT overexpressors as outlined below.

We then extended these studies to begin to examine the ability of the probes to detect regions of demyelination in the adult murine CNS. To address this question we initially selected to use the cuprizone model of demyelination. Feeding responsive animals a diet that contains the copper chelator cuprizone for several weeks results in a defined pattern of demyelination in the forebrain that most strongly affects the corpus callosum. Provided the animals are not treated for too long, removal of cuprizone from the diet results in remyelination over a 6-week interval. Such a wide scale demyelination/remyelination represents a useful model with which to initially test probe efficacy.

A. Materials and Methods

A.1 Animal Preparation

SWR/J mice were obtained from Harlan Laboratory, (Oxford, MI). C57BL/6 mice and C3Fe.SWV-Mbpshi/J shiverer mice were obtained from Jackson Laboratory, Bar Harbor, MN, and the Plp-Akt-DD transgenic mice were generated as described previously (Flores et al., 2008; Narayanan et al., 2009). Briefly, the transgenic mice expressing constitutively active Akt (HAAkt308D473D, Akt-DD) driven by the Plp promoter (Wight et al., 1993) were generated and used as a hypermyelinated animal model. Akt cDNA was inserted into the AscI/PacI sites of the modified Plp promoter cassette, and hypermyelination was induced after the Plp promoter/Akt-DD insert was injected into SJL/SWR F1 mice. Positive founders were identified by PCR amplification of tail DNA using IntronSV40F (5'-GCAGTGGACCACGGTCAT-3') and Akt lower (5'-CTGGCAACTAGAAGGCACAG-3') primer sequences. Analyses were done from litter-matched mice in all developmental experiments, and where possible with older animals. In all three studies Plp-Akt-DD9 was used for these studies. The cuprizone mouse model of demyelination was induced by feeding 6-week-old female C57BL/6 mice with a diet of milled mouse chow containing 0.2% of the copper chelator, cuprizone (Sigma-Aldrich; St Louis, MO)

for 6 weeks for maximal demyelination. To facilitate remyelination, the mice were fed normal milled mouse chow.

A.2 Immunohistochemistry

To ensure maximal penetration of the antibodies in these studies we selected to use free-floating sections that permit labeling throughout the sections. For immunohistochemistry with free floating sections, mice were deeply anesthetized with isoflurane and perfused with PBS followed by 4% paraformaldehyde in PBS via the ascending aorta. Brains were excised, incubated for 24 hours in 4% paraformaldehyde at 4ºC, cryoprotected and sectioned (30 μm) with a sliding microtome. Free floating sections were rinsed in 1xPBS (2x5'), then incubated in 1% H2O2/10% Triton, then washed with 1xPBS (3x5'). After incubation with 3% normal goat serum for 60 minutes, the free floating sections were immunostained overnight at 4ºC with rabbit anti-MBP antibody (Chemicon-Millipore, Bedford, MA) 1: 2000 dilution in 3% normal goat serum in 1xPBS, which was followed by one hour incubation at room temperature with IRDye 800CW Goat Anti-Rabbit (LI-COR Biosciences, Lincoln, NE) 1:5000 dilution, then rinsed in 1xPBS (2x5'). The stained sections were covered with fluorescence mounting medium (Vectashield, Vector laboratories). Images of the stained mouse brain sections were acquired on a LI-COR Odyssey infrared imaging system (LI-COR Biosciences, Lincoln, NE).

For immunohistochemistry with fresh frozen sections, mice were deeply anesthetized with isoflurane and perfused with 1XPBS followed by 4% paraformaldehyde in PBS. The brains were removed and fixed in 4% PFA overnight and then in 30% Sucrose solution. The brains were then sectioned at 20 μm. After incubation with 3% normal goat serum in 1xPBS for 60 min, the fresh frozen sections were immunostained overnight at 4ºC with purified mouse antibody monoclonal SMI99 (Covance, Inc. Princeton, NJ) 1: 500 dilution in 3% normal goat serum in 1xPBS, followed by one hour incubation at room temperature with Fluorescein (FITC) AffiniPure Goat Anti-Mouse IgG (H+L) (Jackson ImmunoResearch Laboratories, Inc. West Grove, PA) 1:500 dilution, then rinsed in 1xPBS (2x5'). The stained sections were covered with fluorescence mounting medium (Vectashield, Vector laboratories). Images of the stained mouse brain sections were acquired on a Leica DM5000 inverted microscope (L5 filter, BP 527/30).

For immunohistochemistry with neuronal marker, free floating sections were incubated in 1% H2O2/10% Triton, washed with 1xPBS(3x5'), then immunostained overnight at 4ºC with mouse anti-MAP2 antibody (sigma-Aldrich. Milwaukee, WI) 1: 800 dilution in 3% normal goat serum in 1xPBS, followed by one hour incubation at room temperature with Alexa Flour 488 goat anti-mouse IgG (Invitrogen, Carlsbad, CA) 1:1000 dilution in 3% normal goat serum/1xPBS, then rinsed in 1xPBS (2x5'). The stained sections were covered with fluorescence mounting medium (Vectashield, Vector laboratories). Images of the stained mouse brain sections were acquired on a Leica DM5000 inverted microscope (L5 filter, BP 527/30).

A.3 DBT chemical staining

For DBT staining with free floating sections, mice were deeply anesthetized with isoflurane and perfused with PBS followed by 4% paraformaldehyde in PBS via the ascending aorta. Brains were excised, incubated for 24 hours in 4% paraformaldehyde at 4ºC, cryoprotected and sectioned (30 μm) with a sliding microtome. Free floating sections were incubated in 1% H2O2/Triton-100 for 10 min, incubated in a solution of DBT (1 μM) in 1% DMSO/PBS for 30 min at room temperature, then washed three times with 1xPBS before cover-slipping with fluorescence mounting medium (Vectashield, Vector laboratories). Images were acquired on a LI-COR Odyssey infrared imaging system (LI-COR Biosciences, Lincoln, NE).

For DBT staining with fresh frozen sections, mice were deeply anesthetized with isoflurane and perfused with 1XPBS followed by 4% paraformaldehyde in PBS. The brains were dissected and fixed in 4% PFA overnight and then cryoprotected in 30% sucrose solution. The brains were then sectioned at 20 μm and fresh frozen sections with 20 μm thickness were incubated in 0.1% Triton-100 in 1xPBS for 10 min, which was followed by incubation in a solution of DBT (1mM) in 1% DMSO/1xPBS for 30 min at room temperature. The fresh frozen sections were then washed three times for 5 min each with 1xPBS before cover-slipping with fluorescence mounting medium (Vectashield, Vector laboratories). Images of the stained mouse brain sections were acquired on a Leica DMI6000 inverted microscope (Y5 filter, BP 700/75).

A.4 Co-registration of fluorescent and X-ray images

Images were acquired with a KODAK In-Vivo Multispectral System FX [Carestream Health, Inc., Rochester, NY]. The fur of the mouse was shaved to avoid autofluorescence artifacts. 20 minutes after the i.v. injection of DBT [0.1 mg/kg], the mouse was anesthetized utilizing isoflurane gas. The mouse was positioned on the center of the platen and imaged via fluorescence (excitation 760 emission 790) and X-ray. Vertical Resolution: 885 ppi, horizontal Resolution: 885 ppi.

A.5 Near-infrared fluorescence in vivo imaging

The in vivo near-infrared fluorescence imaging was carried out using a Xenogen IVIS Imaging System 200, Caliper Life Science. Inc., Hopkinton, MA. To avoid the influence of autofluorescence and light scattering due to the fur, all the mice were shaved before the experiment. After the i.v. injection of DBT 0.1 mg/kg, mice were anesthetized utilizing isoflurane gas, The mouse was then positioned on the center of the stage (working temperature 20-40°C) and near-infrared images were acquired by back-thinned, back-illuminated grade 1 CCD, which was thermoelectrically cooled to -90 °C to ensure a low dark current and low noise. The fluorescent filter was set for excitation at 705-780 nm and for emission from 810-885 nm. The experiments were controlled with a Living Image 3.1 (Caliper Life Science. Inc., Hopkinton, MA). Lens: f/2. Field of view: 6.5cmX6.5cm. Imaging Pixels: 2048X2048. Exposure time: 0.5s for all of the images.

A.6 Quantification and statistical analysis

The near-infrared images were evaluated with a Living Image 3.1 from Caliper Life Science. Inc., Hopkinton, MA. All the images used photon as the unit for the quantification, and the images were shown as an overlaid photograph with fluorescence. Statistical analysis was performed using a two-tailed t-test with GraphPad Prism 5, La Jolla, CA.

B. Results

B.1 Fluorescent properties of DBT

DBT is a highly conjugated dibenzothiazol derivative with a structure shown in **Figure 7A**. The fluorescent excitation and emission spectra of DBT were recorded using Varian fluorescent spectroscopy at a concentration of 100 nM in DMSO. As shown in **Figure 7B,** the excitation and emission maxima of DBT are 782 nm and 797 nm, respectively, which are located in the near infrared region (650 nm-900 nm). Previous studies showed that the extinction coefficient of DBT at 780 nm is 43000 $(M\ cm)^{-1}$. The quantum yield of DBT is 0.034 with a lifetime of 1.18 ns (Sevick-Muraca et al., 1997).

B.2 *In vitro* binding studies

The capability of DBT to bind to myelinated regions of the CNS was first examined by fluorescent tissue staining of wild-type mouse brain sections as discussed previously. For comparison, immunohistochemical labeling with myelin-specific MBP antibodies was also conducted. At 1 μM concentration, DBT selectively labeled intact myelin sheaths present in the whole mouse brain, particularly in the corpus callosum and the caudate putman (**Figure 7C**). The pattern of myelin sheaths stained by DBT was virtually identical to the pattern of labeling by MBP antibody (**Figure 7D**). These observations suggest that DBT binds either directly to, or is closely correlated with myelin sheaths *in vitro*.

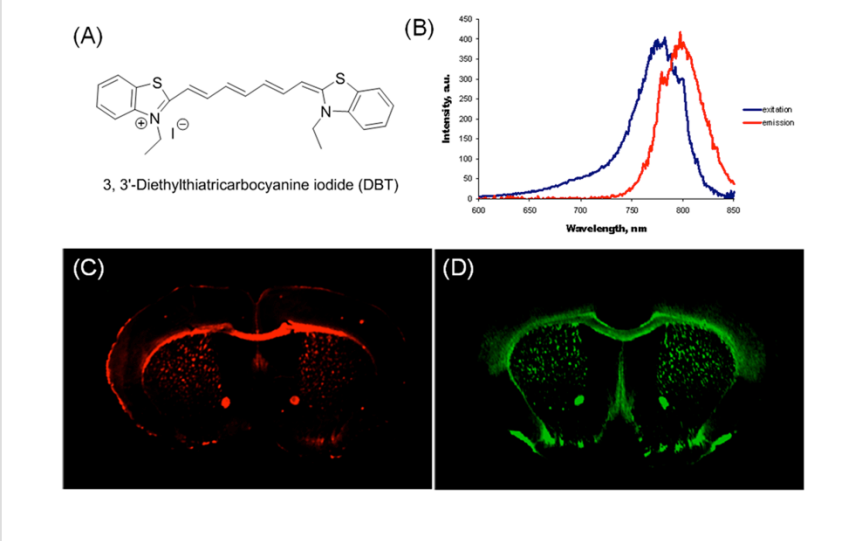

Figure 7. (A) The structure of 3, 3'-Diethylthiatricarbocyanine iodide (DBT); (B) The excitation and emission spectra of DBT (100 nM in DMSO). Excitation spectra: emission at 797 nm (range 600–850 nm), maximal excitation wavelength at 782 nm. Emission spectra: excitation at 782 nm (range 600-850 nm), maximal emission wavelength at 797 nm; (C) *In vitro* DBT staining of free floating brain tissue sections of wild-type mice (1μM); (D) *In vitro* immunohistochemical staining of free floating brain tissue sections of wild-type mice with MBP antibody.

To determine the level of sensitivity of DBT binding detect myelin throughout the neuroaxis, we examined tissue staining by DBT in different brain regions such as caudate putman, cerebellum, and frontal cortex (**Figure 8**, left panels). These regions were selected to represent different forms of myelin fibers in the brain. In the caudate putman, DBT selectively stains compact myelin fibers. In the cerebellum, DBT stains both myelin tracks and surrounding granule layers. In the frontal cortex, DBT can also stain the small myelin fibers that are primarily located in the gray matter regions. These studies suggested that DBT has a high level of sensitivity for myelin specifically and not just white matter tracts since it not only binds to myelin fibers present in the white matter, but also to small bundles of myelin present in the gray matter.

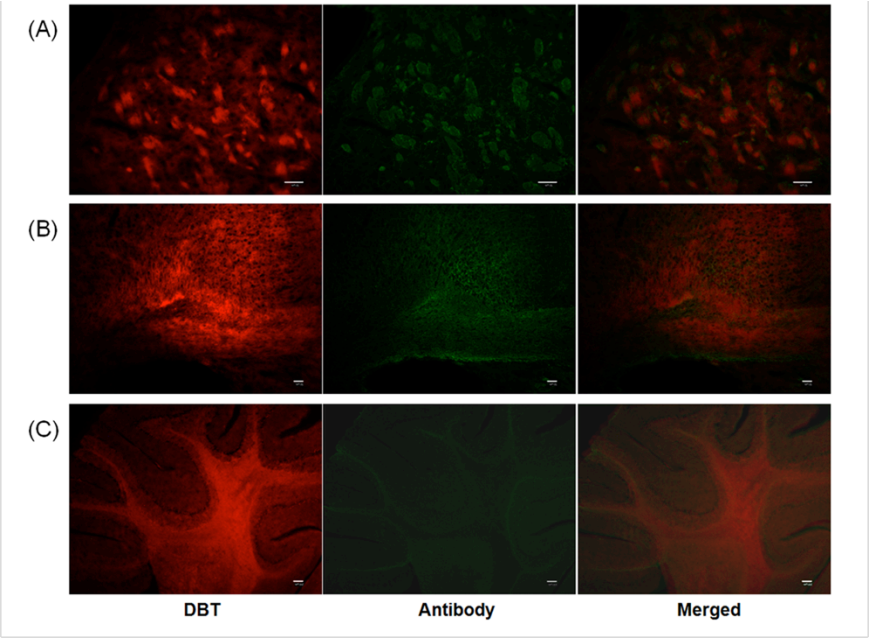

Figure 8. *In vitro* DBT staining of myelinated regions (left panels) and subsequent co-staining of MBP antibodies (middle panels). A: DBT staining of compact myelin fibers present in caudate putamen, which significantly blocks antibody staining of MBP in the same section. B. DBT staining of small myelin fibers present in frontal cortex, which also significantly blocks antibody staining of MBP in the same section. C. DBT staining of both myelin tracts and granule layers present in cerebellum, which significantly blocks antibody staining of MBP in the same section. Inhibition of immunohistochemical staining by DBT indicates that DBT stains myelin through specific binding to MBP. Scale bar: A, B = 50 μm, C = 200 μm.

To define in more detail the binding sites of DBT, a competitive binding assay was developed in which both DBT and MBP staining were conducted in the same brain tissue sections. Each section was first subjected to DBT staining followed by antibody staining of MBP (**Figure 8,** middle panels). The antibody staining was significantly blocked by DBT in different regions including caudate putman (**Figure 8A)**, cerebellum (**Figure 8B)**, and frontal cortex (**Figure 8C)** suggesting that DTB binds directly to myelin possibly to epitopes on MBP.

As a further validation of the system, we conducted tissue staining of DBT in the hypermyelinated Akt and hypomyelinated shiverer mouse brains in comparison with wild-type mouse brains. The myelin staining of the corpus callosum region in each model is shown in **Figure 9A-F**. Compared to the corpus callosum present in the wild-type mouse brain (**Figure 9A** and **9B**), DBT staining of the same region showed significant myelin enrichment in the hypermyelinated Akt mouse brain (**Figure 9C** and **9D**) and was diminished in the shiverer mouse brain (**Figure 9E** and **9F**), which is consistent with their previously defined pathological findings.

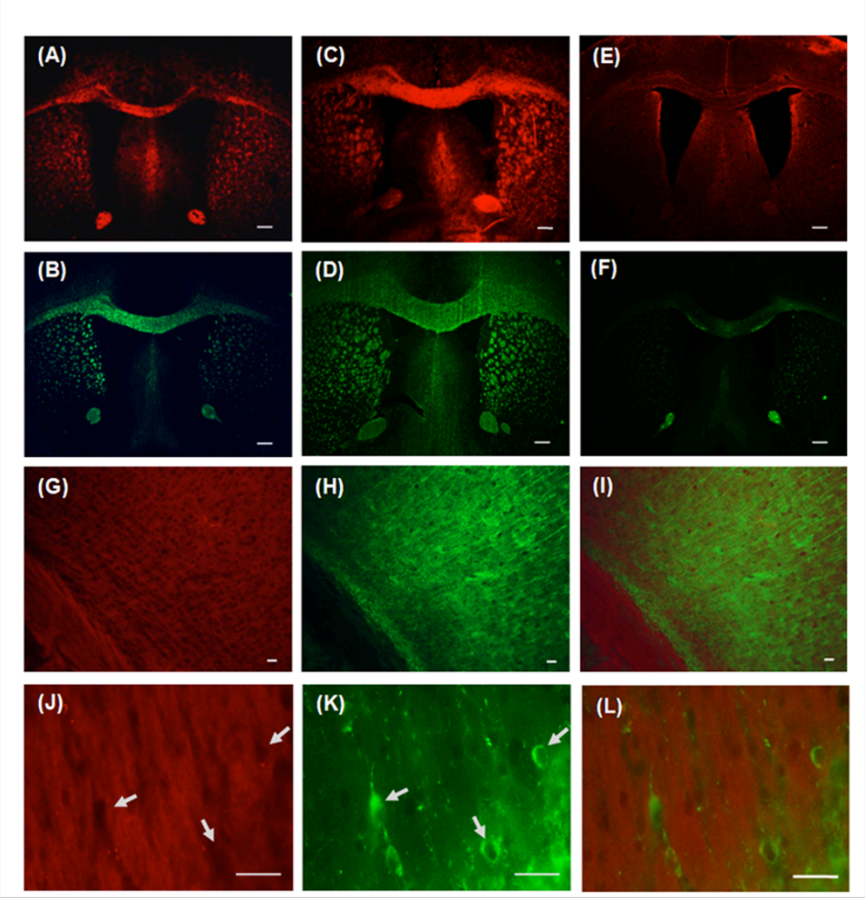

Figure 9. *In vitro* DBT staining and MBP antibody staining of corpus callosum in mouse brain tissue sections of wild-type (A, B), hypermyelinated Akt mouse mutant (C, D), and hypomyelinated shiverer mouse mutants (E, F). *In vitro* double staining of the corpus callosum and subcortical gray matter using MAP2 antibody (H) and DBT (G), with the merged images in 20X shown in (I). Examination of the gray matter at high magnification (40X) to identify subcortical myelinated structures by DBT staining (J) and individual neurons (arrows) by MAP2 staining (K). Lack of DBT staining on some individual neurons is highlighted by arrows with the merged images shown in (L). Scale bar: A-F = 300 μm, G-L = 50 μm.

To examine whether DBT binds to neurons, we conducted double staining for neuronal markers similar to that previously described for MBP. Thus, immunohistochemical labeling of floating mouse brain tissue sections for MAP2 followed DBT staining of the same sections. Images in both low and high magnification of the corpus callosum and subcortical regions were taken separately with the red and green channels. In the 20X images as shown in **Figure 9H-I**, the DBT staining was localized to both the corpus callosum and subcortical gray matter (**Figure 9G**) while the MAP staining was largely confined to the subcortical region (**Figure 9H**). When the subcortical region was examined at a higher magnification (40X) to identify individual neurons as shown in **Figure 9J-L**, individual neurons were clearly visualized by MAP2 staining (**Figure 9K**), but were not labeled with DBT, which was localized only to the subcortical myelinated structures (**Figure 9J**), suggesting that DBT selectively binds to myelin, but not to neurons. Further, no specific binding of DBT was detected on mouse forebrain dissociated cell cultures consistent with the binding specificity of DBT for myelin (results not shown).

B. 3 Brain permeability

To determine the permeability of DBT to the CNS following systemic delivery, we administered DBT to wild-type mice through intravenous injection in the tail vein. At 20 minutes post injection of DBT (0.1 mg/kg), both X-ray and fluorescent images of the mouse brain were acquired using a KODAK In-Vivo Multispectral System FX **(Figure 10).** Co-registration of the high quality X-ray image and fluorescent image confirmed that the strong fluorescence was indeed emitted from inside the brain. The results indicate that DBT can readily penetrate the intact blood-brain barrier, making it a suitable NIR probe for *in vivo* studies.

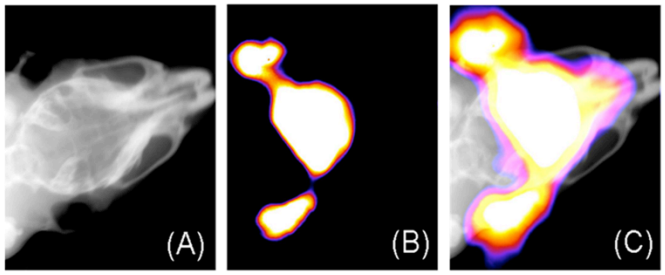

Figure 10. The X-ray image (A) and fluorescent image (B) of a living wild-type mouse from Kodak multispectral imaging system. The precise overlay image without fiduciary markers is shown in C.

B.4 *In vivo* NIRF imaging of myelin

In vivo NIRF imaging was conducted in three mouse models that reflect different levels of myelination in the brain. Female 3-month old *Plp-Akt*-DD mice (n=3) were used to represent hypermyelination in the brain. Age-matched Swiss Webster wild-type mice (n=2) were used to represent intact, normal myelination in the brain. Shiverer mice (C3Fe.SWV-Mbp^{shi}/J and n=2) were used to represent deficient myelination in the brain.

1) *In vivo* NIRF imaging in a hypermyelinated mouse model

DBT (0.1 mg/kg) and vehicle (0.05% DMSO/PBS (V/V) were first administered to the hypermyelinated mouse models through intravenous injections in the tail vein. The fluorescence signals were recorded at 2, 4, 6, 8, 10, 15, 20, 25, 30, 40, 50, 60, 70, 80, 90, 100, 110 and 120 minutes post-injection. The images recorded at 2, 4, 6, 8, 10, 15, 20, 25, 30 minutes post-injection are shown in **Figure 11.** To exclude the influence of autofluorescence from the mouse tissues and impact from the solution, the vehicle (0.05% DMSO/PBS (V/V) was also injected and fluorescence was recorded at 2, 4, 6, 8, 10, 15, 20, 25, 30, 40, 50, 60, 70, 80, 90, 100, 110 and 120 minutes to compare with the DBT solution (images not shown). The fluorescent radiance of *Plp-Akt*-DD mice is much stronger than that observed in the wild-type mice, which is consistent with the fact that the myelin content in the *Plp-Akt*-DD mice is much higher than that in the wild-type mice.

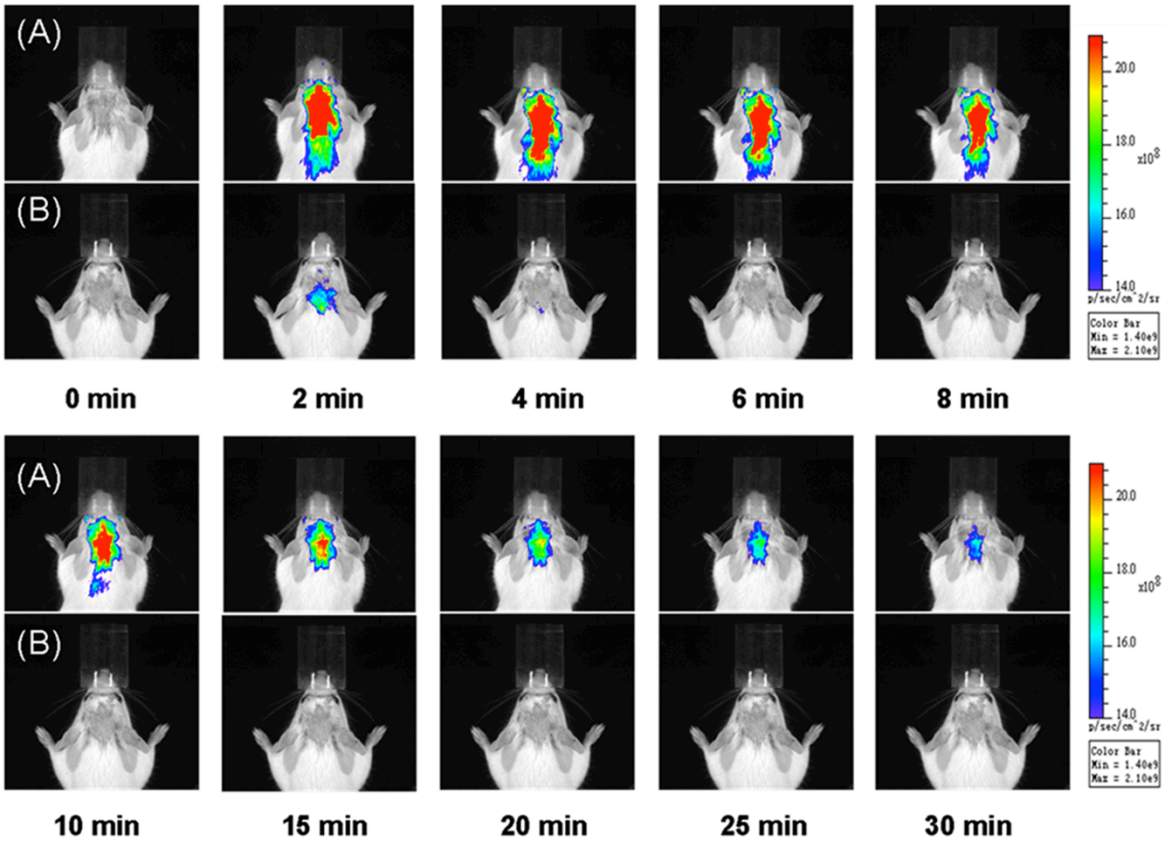

Figure 11. Near-infrared fluorescence *in vivo* imaging in Plp-Akt-DD mice (A) and wild-type mice; (B) recorded at 0, 2, 4, 6, 8, 10, 15, 20, 25, 30 minutes after the i.v. injection of DBT 0.1mg/kg.

Quantitative analysis of these images was then conducted as shown in **Figure 12.** Over a period of 30 minutes, the average fluorescent intensity of DBT in *Plp-Akt*-DD mice is fourfold higher than that observed in wild-type mice. This is consistent with the enhanced myelin content in *Plp-Akt*-DD mice. The significant difference between the hypermyelinated and wild-type models appeared as early as 2 minutes post injection with a much stronger fluorescent signal being detected in the hypermyelinated mouse brain, indicating facile brain entry of DBT in proportion to the myelin content. Compared to the fast clearance of DBT in the WT control, relatively slower clearance was observed in the hypermyelinated mice. These results show the potential of DBT used as a probe for *in vivo* near-infrared fluorescence imaging.

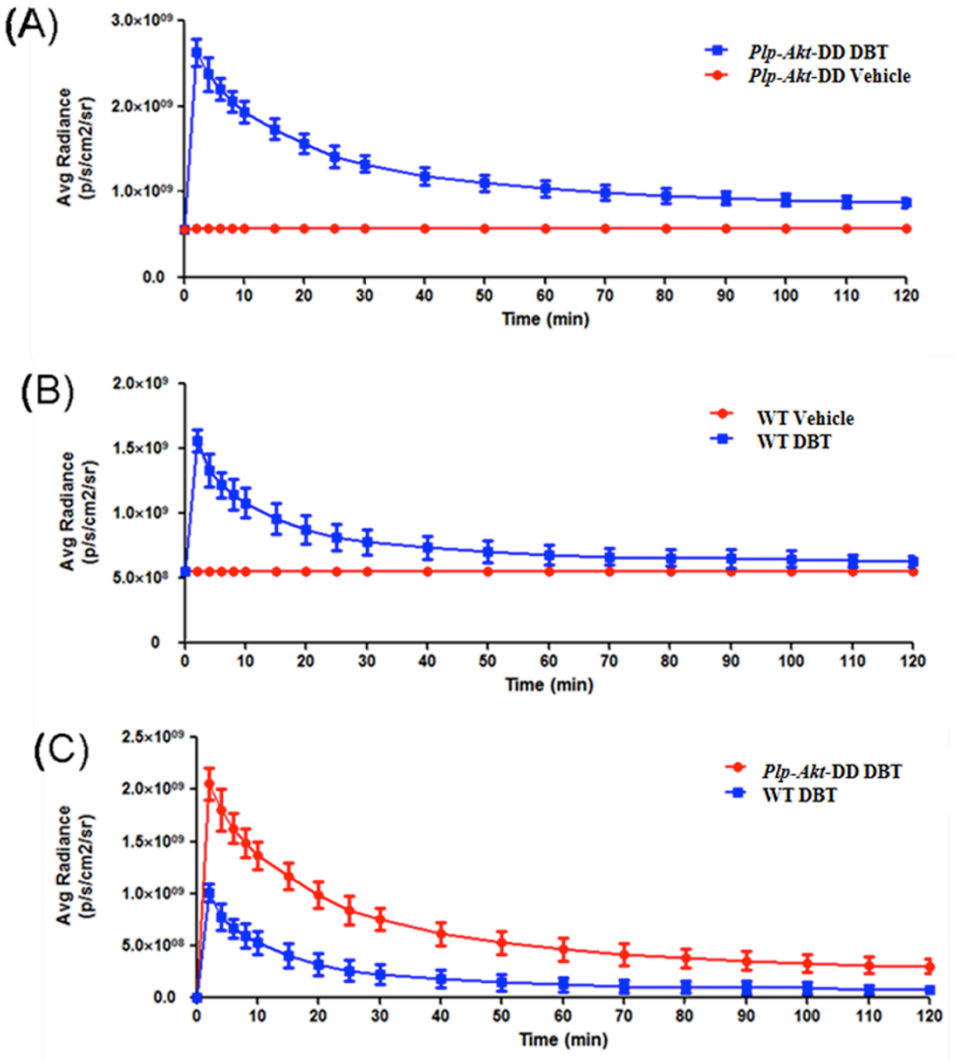

Figure 12. Quantification of *in vivo* imaging of the myelin sheath in living mice. (A) The average radiance of Plp-Akt-DD mice after the injection of DBT (blue) and vehicle (red) at 0, 2, 4, 6, 8, 10, 15, 20, 25, 30, 40, 50, 60, 70, 80, 90, 100, 110, 120 minutes ($P<0.0001$, two-tailed t-test, CI 99%). (B) The average radiance of wild-type mice after injection of DBT (blue) and vehicle (red) at 0, 2, 4, 6, 8, 10, 15, 20, 25, 30, 40, 50, 60, 70, 80, 90, 100, 110, 120 minutes ($P<0.0001$, two-tailed t-test, CI 99%). (C) Comparison of the average radiance between the Plp-Akt-DD mice (red) and wild-type mice (blue) after deducting the vehicle signals ($P=0.0012$, two-tailed t-test, CI 99%). Values are given as mean ±SD.

2) *In vivo* NIRF imaging in shiverer mouse model

We then evaluated the pharmacokinetic profiles of DBT in 3-month old female shiverer mice (n=3) and age-matched wild-type mice (n=2). *In vivo* NIR imaging was conducted using the same dosage as in the hypermyelinated mouse models. The fluorescent signals were recorded at 2, 4, 6, 8, 10, 15, 20, 25, 30, 40, 50, 60, 70, 80, 90, 100, 110 and 120 minutes after i.v. injection of DBT and the vehicle (0.05% DMSO/PBS (V/V)). As shown in **Figure 13**, the fluorescent

intensities in the brain between the two shiverer and wild-type models were significantly different.

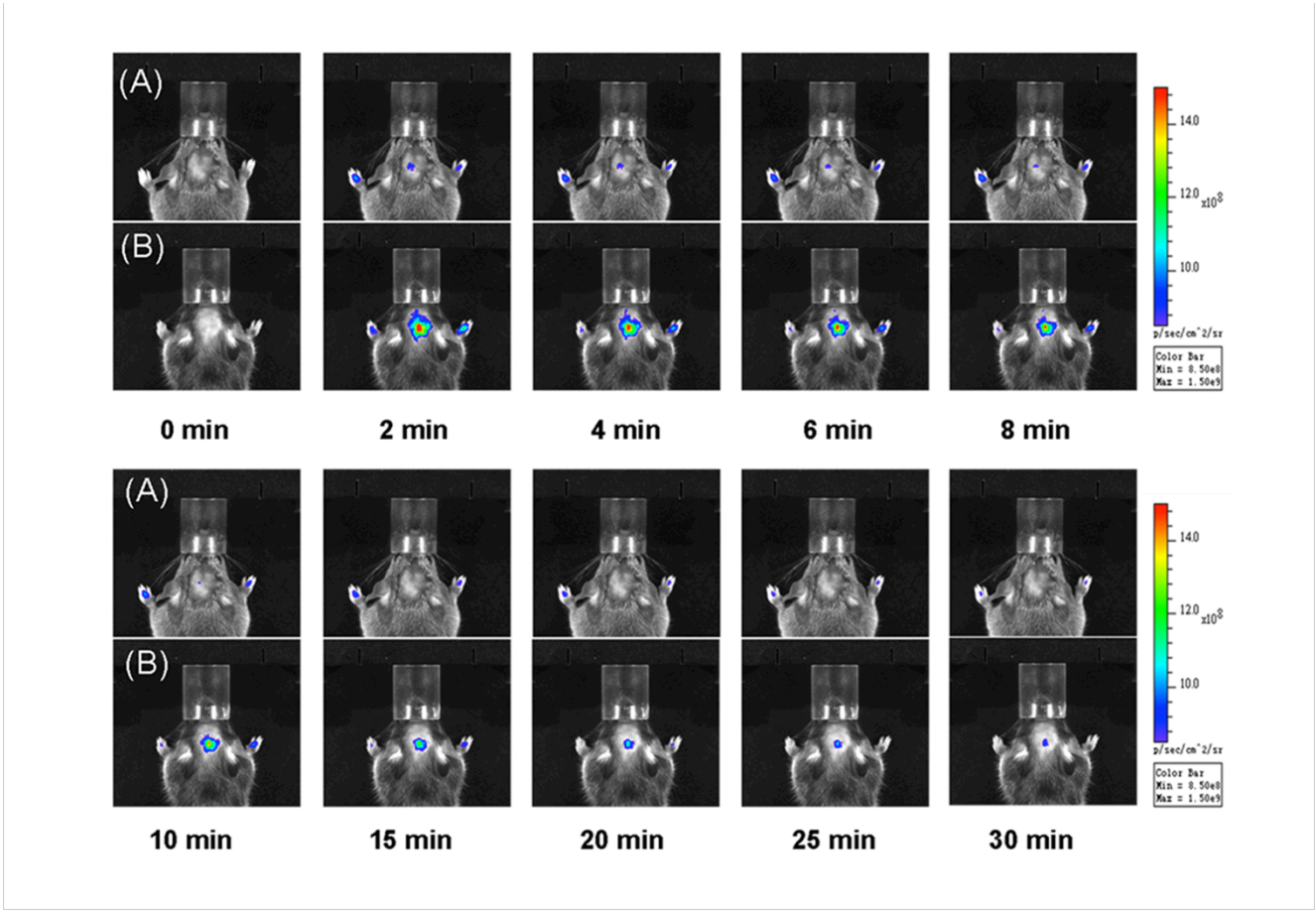

Figure 13. Near-infrared fluorescence *in vivo* imaging in shiverer mice (A) and wild-type mice (B) recorded at 0, 2, 4, 6, 8, 10, 15, 20, 25, 30 min after i.v. injection of DBT 0.1mg/kg.

Based on these images, quantitative analyses were conducted to determine the time course of fluorescent radiance. As shown in **Figure 14**, the average radiance at 30 minutes in wild-type mice is eight fold greater than that observed in shiverer mice. Since shiverer mice are deficient in CNS myelin, the fluorescent signal originating from shiverer mice is very weak, even at its peak at 2 minutes. These results further demonstrated that accumulation of DBT in the brain is proportional to the myelin content and can be used as a surrogate marker of myelination.

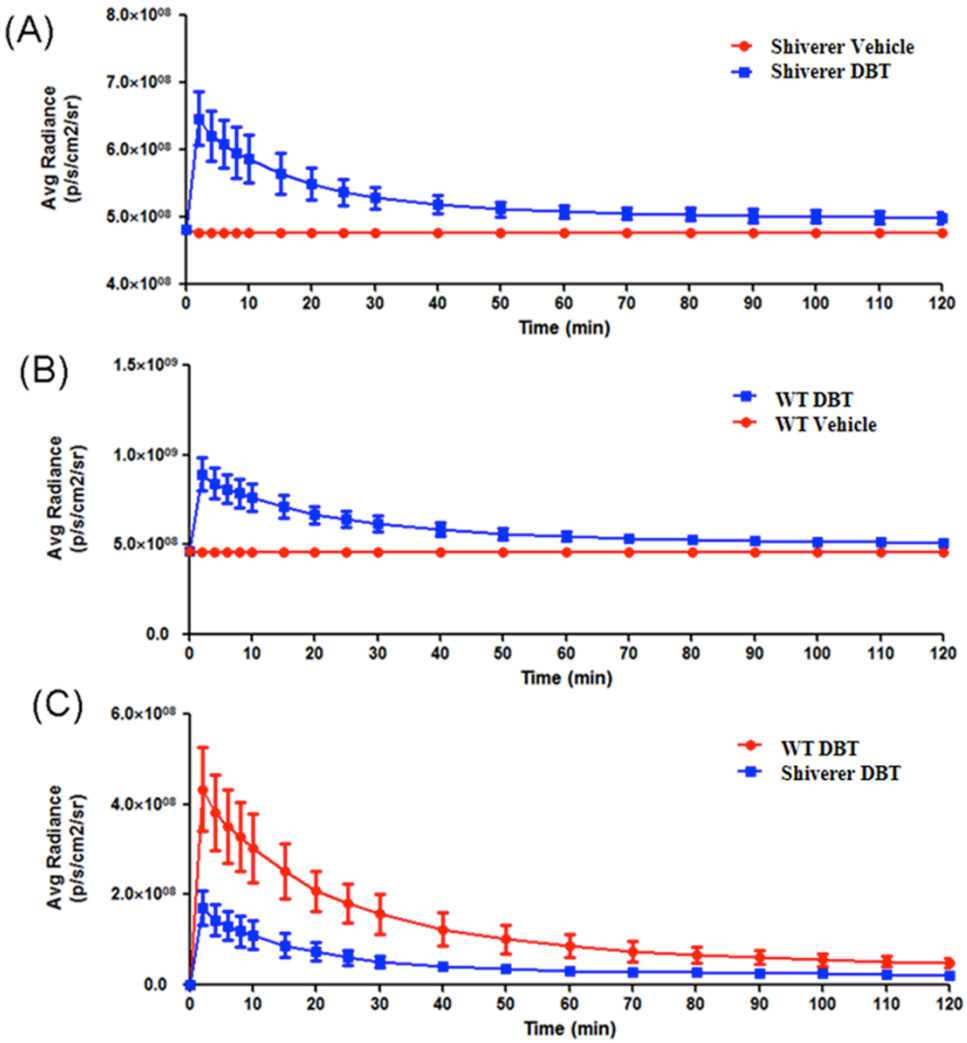

Figure 14. The quantification of *in vivo* imaging of the myelin sheath in the living mice. (A) The average radiance of shiverer mice after the injection of DBT (blue) and vehicle (red) at 0, 2, 4, 6, 8, 10, 15, 20, 25, 30, 40, 50, 60, 70, 80, 90, 100, 110, 120 minutes ($P<0.0001$, two-tailed t-test, CI 99%). (B) The average radiance of wild-type mice after the injection of DBT (blue) and vehicle (red) at 0, 2, 4, 6, 8, 10, 15, 20, 25, 30, 40, 50, 60, 70, 80, 90, 100, 110, 120 minutes ($P<0.0001$, two-tailed t-test, CI 99%). (C) The comparison of the average radiance between the shiverer mice (blue) and wild-type mice (red) after deducting the vehicle signals ($P=0.0019$, two-tailed t-test, CI 99%). Values are given as mean ±SD.

3) Longitudinal NIRF imaging of myelin changes in a cuprizone-induced mouse model of demyelination and remyelination

We then conducted longitudinal NIRF imaging studies in a cuprizone-treated mouse model of demyelination and remyelination at the 6th week of demyelination and the 4th and 8th week of remyelination. The longitudinal NIRF imaging was conducted using the same dosage as previously used in other mouse models. Fluorescent signals were recorded at 5, 10, 15, 20, 25,

30, 40, 50, 60, 70, 80 and 90 minutes after i.v. injection of DBT (**Figure 15)**. Quantitative image analyses were then conducted to determine the time course of fluorescent radiance detected using the whole brain as region of interest (**Figure 16A**). Compared to wild-type control brains, the fluorescent intensity was significantly reduced in the same mouse brains following 6 weeks of cuprizone treatments. The mice were then allowed to recover with normal diets for up to 8 weeks. At the 4th week of recovery, the fluorescent intensity was increased, which was slightly above the level detected after 6-weeks of demyelination. At the 8th week of recovery, the fluorescent intensity was further increased, yet still below the level detected in the normal control brains. After imaging, mice were sacrificed by perfusion and immunochemical staining was conducted on the frozen sections to examine the lesion load in the corpus callosum at different time points. As shown in **Figure 16B-E**, immunochemical staining suggested that the lesion loads at each time point were consistent with the optical imaging results. Compared to the peak of demyelination, the myelin content was gradually increased at the 4th week and 8th week of remyelination. Yet, the myelin content was still significantly below the level present in the normal control brain as previously demonstrated by others. These results demonstrated that DBT is a sensitive marker of myelin that is capable of longitudinal monitoring of myelin content in vivo.

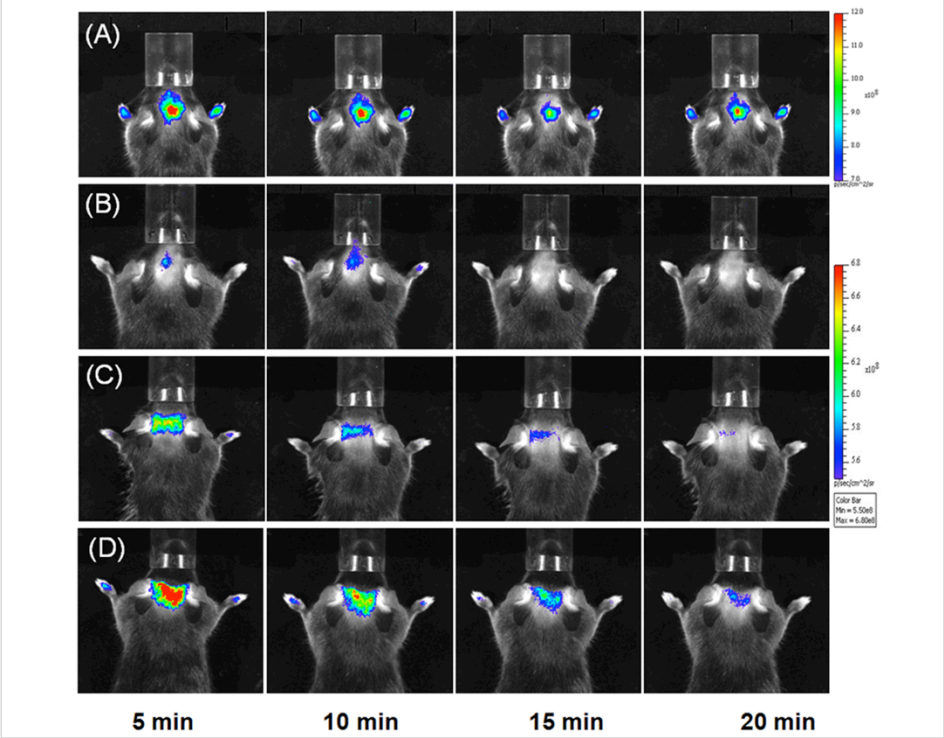

Figure 15. Representative *in vivo* near-infrared fluorescence images in a normal control mouse brain (A) mouse brain treated with cuprizone for 6 weeks (B), cuprizone-treated mouse brain after remyelination for 4 weeks (C), and cuprizone-treated mouse brain after remyelination for 8 weeks (D). NIRF images of each mouse brain were recorded at 5, 10, 15, 20 minutes after the i.v. injection of 0.1mg/kg of DBT.

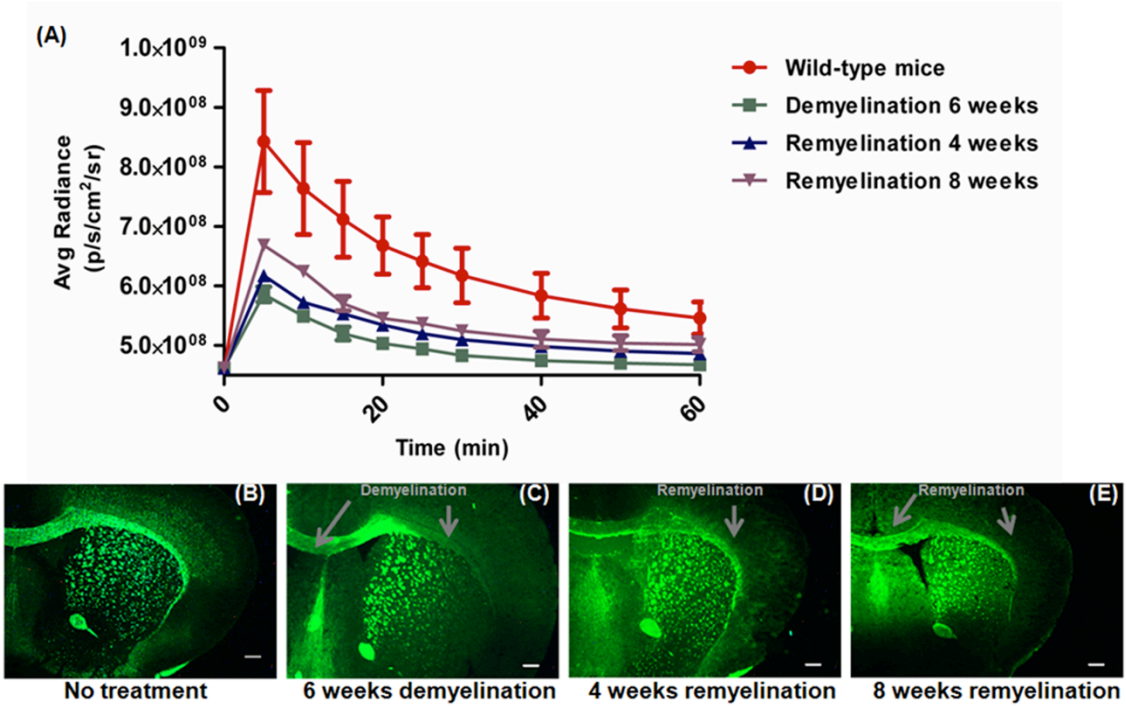

Figure 16. (A) Quantification and comparison of fluorescent intensity detected in mouse brains after NIRF imaging in different mouse models. The time courses of the average radiance of DBT detected in normal control mouse brain (red), mouse brain treated with cuprizone for 6 weeks (green), cuprizone-treated mouse brain after remylination for 4 weeks (blue) and cuprizone-treated mouse brain after remylination for 8 weeks (purple) (P=0.0006, one-way ANOVA test, CI 95%). Value are given as mean ±SD; (B-E) After imaging, corresponding immunochemical staining was conducted at different stages including wild-type (B), cuprizone-induced demyelination (C), remyelination of 4 weeks (D), and remyelination of 8 weeks (E). Scale bar: 300 μm.

C. Discussion

Taking advantage of the inherent fluorescence, the binding specificity of DBT for myelin was first evaluated through tissue staining of mouse brain sections. As shown in **Figure 7**, myelinated regions such as corpus callosum and caudate putman were selectively labeled by DBT. To determine which forms of myelin fibers can be stained by DBT, we further examined tissue staining of additional brain regions in both white matter and gray matter including the cerebellum and frontal cortex. As shown in **Figure 8**, in addition to the binding of compact myelin fibers present in the caudate putman, DBT stains granule layers present in the cerebellum. More interestingly, DBT also stains small myelin fibers present in the frontal cortex. Following DBT staining, subsequent immunohistochemical staining of MBP was significantly reduced or even completely blocked, which suggests that DBT binds to MBP present in the myelin sheaths and stains both compact myelin fibers and small myelin fibers. The binding specificity of DBT for myelin was further validated by tissue staining in relevant areas of the hyper- and hypomyelinated mouse mutants as well as immunohistochemical staining of neurons (**Figure 9**). These studies indicated that DBT is a small molecular probe that is sensitive and specific for all

the forms of myelin present in the CNS. This is the first time that a small molecular probe has been developed with a myelin-binding property similar to MBP antibody.

To examine the sensitivity and specificity *in vivo*, we conducted *in vivo* DBT-NIRF imaging in two animal models. The *Plp-Akt*-DD model was used to represent a myelin-rich state while the shiverer mouse model was used to represent a myelin-deficient state relative to wild-type controls. At 2 minutes after tail vein injection, strong fluorescent signals were detected in the hypermyelinated *Plp-Akt*-DD mouse model relative to the wild-type under the same attenuation power (**Figure 11**). To confirm that the fluorescent signals were from inside the brain, the fluorescent images were co-localized with the corresponding X-ray images, which were used to define the brain region (**Figure 10**). Quantitative analysis of the fluorescent intensity showed that DBT retention in the *Plp-Akt*-DD mouse brain is significantly higher than that in the wild-type control (**Figure 12**). In contrast, opposite results were observed in myelin-deficient shiverer mice. The fluorescent signals were relatively weak in the shiverer mice after tail vein injection compared to the wild-type controls under the same attenuation power (**Figure 13**). Quantitative fluorescent intensity showed that DBT retention in the shiverer mouse brain is significantly lower than that in the wild-type mouse brain (**Figure 14**). In addition, a dose of DBT as low as 0.1 mg/kg was used in the imaging studies. No animals experienced any adverse pharmacologic effects during these studies. The pharmacokinetic profiles of DBT correlate with the well-defined myelin levels in both mouse models suggesting that DBT-NIRF is a sensitive and specific imaging marker of myelination.

To broaden the application of DBT to MS disease, we then conducted longitudinal imaging studies to monitor demyelination and remyelination in a cuprizone-induced mouse model. In this model, young adult mice are fed with the copper chelator cuprizone (bis-cyclohexanone oxaldihydrazone). This leads to consistent demyelination followed by spontaneous remyelination after the neurotoxin is replaced with normal diets. Based on NIRF imaging and quantitative analysis (**Figure 15**), the fluorescent intensity of DBT can be used to monitor the level of demyelination and subsequent remyelination in the cuprizone model, which correlate well with histochemical staining (**Figure 16**). Thus, DBT-NIRF can be used as an imaging marker of myelination for longitudinal studies of myelin-related diseases in animal models.

Each DBT-NIRF study takes only several hours. After disappearance of the fluorescent signal, the same study can be repeated in the same animals, which can be used for longitudinal studies and fast throughput screening of drugs targeted at myelination. In addition, DBT showed no adverse pharmacological or behavioral effects in vivo when up to 50 mg/kg of DBT were administered through tail vein injection. Thus, DBT-NIRF provides a very economical and practical tool for myelin imaging that complements current imaging modalities.

Specific Aim 2: Analysis of myelin repair in response to selected therapeutic agents monitored by MicroPET Imaging

Major Task 1: Longitudinal imaging of Demyelination and Remyelination in spinal cord following Mesenchymal Stem Cells (MSC) Treatment

Rationale: while the previous studies provide strong evidence that the probes developed in this program have the capability to accurately detect changes in the level of myelination in distinct mouse mutant and to reveal changes in myelination in the cuprizone model, the ultimate goal of the project is to use the capabilities of the probes to detect changes in the level of myelination in patients undergoing distinct therapeutic regimes for MS. This capability becomes incredibly important given that emerging data suggests there is heterogeneity in the pathobiology of MS

and in the likely responses of individual to single treatment regimes. With the emergence of therapies targeted towards myelin repair, it is essential that non-invasive, longitudinal methods of measuring myelin levels be developed. To begin to assess the capability of the CIC to detect therapy induced myelin repair we have utilized the local lesion model induced by injection of the gliotoxin into the dorsal spinal cord. This model generates a reproducible lesion that undergoes a stereotyped repair and the effect of therapies on that repair process can be effectively monitored at the histological level.

A. Material and Methods:

A.1 Preparation of LPC model of focal demyelination in the spinal cord

To produce a focal demyelinating lesion a laminectomy was performed on adult female Sprague Dawley rats at the level of the thoracic spinal cord (T13). Using a pulled glass needle 1.5ul of a 1% solution of lysophosphatidylcholine (LPC) was injected into the spinal cord at a depth of 0.5mm over a period of 5minutes and the needle withdrawn slowly. The overlying muscle was sutured back in place and the skin and dermal layers stapled. All procedures were done under sterile conditions and the lesion site treated with betadine solution. Animals were maintained on a heating pad and monitored daily. No significant functional impairment was noted in any animal.

A. 2 HGF treatment

Animals were randomly assigned to experimental and control groups and treated with 0.4 or 0.8µg/Kg HGF (n=8) or saline (n=6) iv through a tail vein on days 4, 6 and 11 and the animals sacrificed for histological analyses on days 14 and 21 post lesion. Preliminary studies indicated a more robust remyelination response to the higher concentration of HGF and this was used in all subsequent studies. Analyses of the extent of demyelination and remyelination was performed on 20mm thick sections stained with Luxol fast blue and confirmed by immunohistochemical labeling with antibodies to myelin basic protein to detect oligodendrocytes, NG2 to detect oligodendrocyte precursors and Glial fibrillary Protein to detect astrocytes. The extent of demyelination and myelin repair was confirmed through analyses of 1mm plastic embedded sections stained with Toluidine Blue and at the EM level on thin sections stained with Uranyl acetate and lead citrate and visualized in a Jeol 100X microscope with and accelerating voltage of 100Kv.

B. Results and Discussion

Remyelination in the LPC lesion

The lesion that is induced by LPC injection can be monitored histologically and at the ultrastructural level Figure 17. The lesion can be seen in the dorsal white matter of the spinal cord in cross-sections labeled with luxol fast blue. The extent of the lesion is detected with concomitant injection of dye and the demyelinated region can be reconstructed in three dimensions from serial sections. At higher magnification the lack of myelin within the lesion is detectable by luxol fast blue staining and therapeutic enhancement of remyelination can be detected both by luxol staining (Middle panel) and at the ultrastructural level.

We have used a combination of EAE studies and LPC studies to define potnetial myelin reapir therapies. One of the most promising is treatment with Meschymal Stem Cells MSC which in the setting of EAE promote rapid recovery see **Figure 17**. This model which is based on an immunologial inisult is not the best for studying remyelination since there is ongoing demyelination and remylination, but it does show the effeciacy of the treatment with MSCs

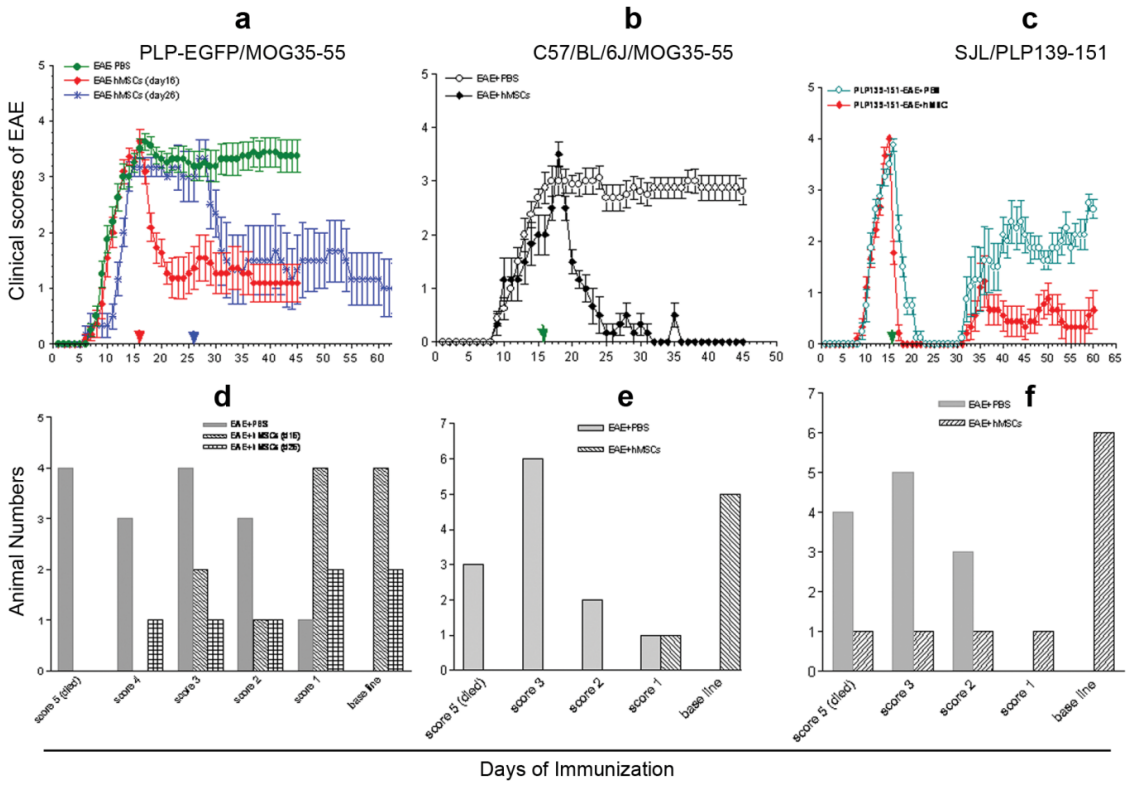

Figure 17. Treatment with human MSCs in 2 models of EAE results in a rapid and profound functional recovery. This recovery is correlated with histological improvement.

To begin to use the imaging probes effectively with therapeutic intervention we first sought to identify the active signals from MSCs. Current studies suggest this is Hepatocyte Growth Factors and these studies are currently ongoing. Thus, we utilized a different lesion model to study the effects of HGF on remyelination using Dr. Wang's probes.

We selected to use the LPC lesion discussed above.

Characterization of the LPC lesion. Figure 18

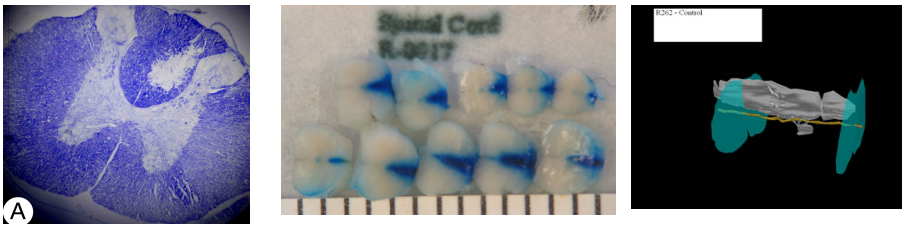

Control Remyelinating EM

Figure 18 Top: The characteristics of the LPC lesion in the dorsal spinal cord. Bottom: Measurement of repair in histological sections both Luxol and EM.

This year we have started to use imaging to longitudinally monitor the efficacy of mesenchymal stem cells (MSCs) derived HGF in promoting remyelination and this will be a major focus of the coming year. Following radiolabelling with positron-emitting carbon-11, [^{11}C]CIC-PET was conducted in longitudinal studies using a lysolethicin-induced rat model of focal demyelination and subsequent remyelination. Quantitative analysis showed that the retention of [^{11}C]CIC correlates with the level of demyelination and remyelination in the spinal cord. These studies indicate that [^{11}C]CIC-PET can be used as an imaging marker of myelination. The ability to image endogenous myelin and quantify demyelination and remyelination with a high degree of spatial and temporal reolution is unique to this approach, which has the potential to be translated into clinical studies in MS and other myelin-related diseases for early diagnosis, sub-typing, and efficacy evaluation of therapeutic treatments aimed at myelin repair.

As shown in **Figure 19**, [^{11}C]CIC-PET is capable to detect and quantify both demyelination and remyelination. The level of [^{11}C]CIC uptake was found to be in the same order of increasing myelin contents as presented in the demyelinated, remyelinated, and intact control stages, respectively. In this study, demyelination was induced to the spinal cord, which was selected as the region of interest (ROI) for comparison. The uptake of [^{11}C]CIC in LPC spinal cord treated with PBS was found to be less than that treated with HGF present in the mesenchymal stem cells. After two weeks of HGF treatment, the uptake of [^{11}C]CIC was significantly increased, which was consistent with the pathological findings based on immunochemical staining. In the coming year we will directly quantify the relative levels of myelin repair using CIC labeling in combination with luxol staining and ultrastructural studies

Following imaging studies, all of the animals survived and showed no signs of any behavioral changes, indicating the radioligands have no apparent toxicity. The robust differentiation between demyelination and remyelination clearly demonstrated the feasibility of using [^{11}C]CIC-PET to quantify myelin changes *in vivo* in animal models. For the first time, it provides a powerful tool for drug screening at preclinical stage to directly monitor time course of myelin changes.

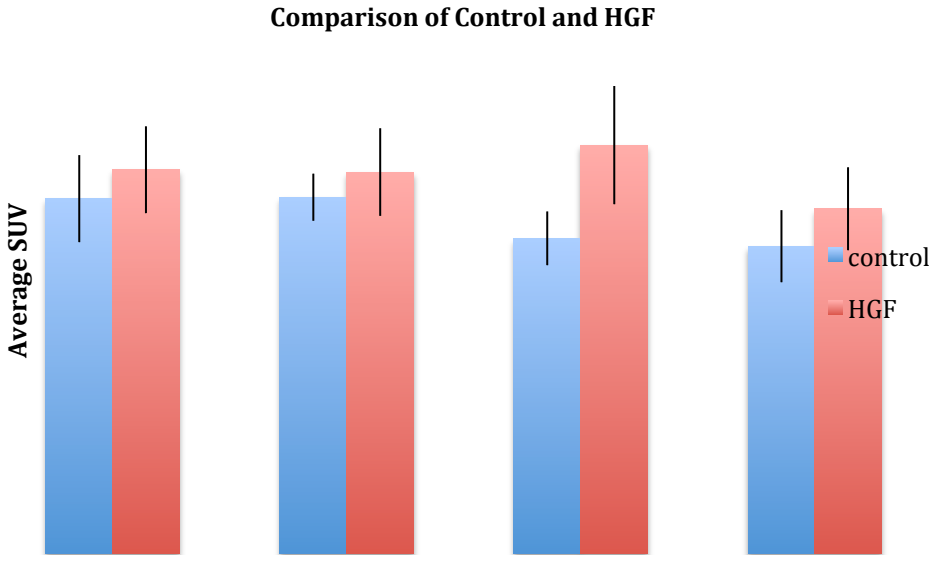

Figure 19. [^{11}C]CIC-PET imaging of the LPC-treated spinal cord in rats. LPC-spinal cord were treated with HGF vs PBS over 3 weeks. Quantitative analysis showed that at day 14, HGF treatment makes the

biggest difference in comparison with the PBS treatment. The quantitative analysis was coducted using the same region of interest that was previously defined around the injection point of the spinal cord.

Key Research Accomplishments

During the first funding cycle, we first further optimized the imaging techniques by developing some additional myelin imaging agents. We then conducted longitudinal studies in animal models of MS following therapeutic treatments. The key research accomplishments are highlighted below:

1. A series of myelin-imaging compounds have been synthesized for optimization
2. A lead compound termed FCP has been identified suitable for PET imaging of myelination
3. An imaging agent termed DBT has been identified suitable for both PET and optical imaging
4. DBT has been evaluated through systematic tissue staining
5. DBT has been used for longitudinal imaging studies
6. LPC model of focal demyelination in the spinal cord has been successfully prepared.
7. The mice have been subsequently treated with mesenchymal stem cell (MSC) derived HGF
8. PET imaging has been successfully conducted

Reportable Outcomes

1. Wang C, Wu C, Zhu J, Miller R.H, Wang YM, (2011) Design, Synthesis and Evaluation of Coumarin-based Molecular Probes for Imaging of Myelination*, Journal of Medicinal Chemistry,* 54(7): 2331-2340.
2. Wang C, Wu C, Popescu D, Zhu J, Macklin W, Miller R.H, Wang YM, Longitudinal Optical Imaging of Myelination Based on Near Infrared Fluorescence, (2011) *Journal of Neuroscience* 31(7):2382-2390*.*

Conclusion

In summary, we have demonstrated that fluorescent coumarin derivatives represented by **32** can be developed as myelin-imaging agents for imaging of myelination in the CNS and nerve mapping in the CNS. In this study, we first show that global lipophilicity is an important factor for brain permeability and binding affinity for myelin. Compounds with a logPoct value between 2.5-4 tend to bind to myelin with high affinity. Further SAR analysis indicated that, when lipophilicity is similar, some other physicochemical properties become the determining factors. Because the binding interaction is likely to take place in a hydrophobic environment, presence of hydrophilic groups such as hydroxyl diminishes the binding affinity. Lower electron density of nitrogen enhances the binding affinity. Through structure-activity studies, we have identified **32,** which readily penetrates the BBB and selectively stained intact myelin sheaths in the brain. **32** can also be used as a fluorescent probe for intraoperative nerve mapping in the PNS. In addition, **32** is capable of radiolabeling with F-18, thus making it a promising candidate as PET radiotracer for routine clinical studies, which will be primary focus for future investigations.

Subsequently, we demonstrated that DBT is a promising probe for near infrared fluorescence imaging of myelination in vivo. It readily enters the brain and selectively binds to myelin

sheaths. *In vivo* NIRF studies in animal models of both hypermyelination and hypomyelination showed that DBT-NIRF is a sensitive and specific imaging marker of myelination.

We also developed the lysolecithin (LPC) model to characterize demyelination and remyelination and monitor therapeutic efficacy of MSC treatment using microPET analysis in the spinal cord of the rat. Further studies are on the way to determine whether MSC efficacy will be uniformly beneficial across different animal models. Following MSC treatment, microPET analysis, functional readout, and ultimately histological characterization will be conducted on these animals. We will also conduct a dose escalation study to determine whether increased dosage of human MSCs result in beneficial outcomes.

References

Sherman DL, Brophy PJ (2005) Mechanisms of axon ensheathment and myelin growth. Nat Rev Neurosci 6:683-690.

Hildebrand C, Remahl S, Persson H, Bjartmar C (1993) Myelinated nerve fibers in the CNS. Prog Neurobiol 40:319-384.

Hauw JJ, Delaere P, Seilhean D, Cornu P (1992) Morphology of demyelination in the human central nervous system. J Neuroimmunol 40:139-152.

Compston A, Coles A (2002) Multiple sclerosis. Lancet 359:1221-1231.

Wallin MT, Page WF, Kurtzke JF (2004) Multiple sclerosis in US veterans of the Vietnam era and later military service: race, sex, and geography. Ann Neurol 55:65-71.

Molyneux PD, Barker GJ, Barkhof F, Beckmann K, Dahlke F, Filippi M, Ghazi M, Hahn D, MacManus D, Polman C, Pozzilli C, Kappos L, Thompson AJ, Wagner K, Yousry T, Miller DH (2001) Clinical-MRI correlations in a European trial of interferon beta-1b in secondary progressive MS. Neurology 57:2191-2197

Appendices

1. Wang C, Wu C, Zhu J, Miller R.H, Wang YM, (2011) Design, Synthesis and Evaluation of Coumarin-based Molecular Probes for Imaging of Myelination*, Journal of Medicinal Chemistry,* 54(7): 2331-2340.
2. Wang C, Wu C, Popescu D, Zhu J, Macklin W, Miller R.H, **Wang YM**, Longitudinal Optical Imaging of Myelination Based on Near Infrared Fluorescence, (2011) *Journal of Neuroscience* 31(7):2382-2390.

STATEMENT OF WORK – 11/1/2010-10/30/2011

Site 1: Case Western Reserve University
Org#1 Department of Radiology
PI: Yanming Wang

Site 2: Case Western Reserve University
Org #2 Department of Neuroscience
Partnering PI: Robert Miller

Specific Aim 1(specified in proposal)	Timeline	Site 1	Site 2
Major Task 1: Obtain 8-week old C57BL/6 mice and C3Fe.SWV-Mbpshi/J shiverer mice for optimization of myelin imaging agents through tissue staining	months		
Subtask 1 **Chemical Synthesis**	1-4 months	Dr. Wang	
Subtask 2 **Animal preparation and tissue processing (12 animals)**	1-4 months		Dr. Miller
Subtask 3 **Chemical staining**	2-4 months	Dr. Wang	
Subtask 4 **Immunohistochemistry**	1-4 months		Dr. Miller
Subtask 5 **Black-Gold II staining**	2-4 months		Dr. Miller
Subtask 6 ***In situ* tissue staining of normal control mice brain section**	3-4 months	Dr. Wang	
Subtask 7 ***In vivo* visualization of PNS nerves**	4-6 month	Dr. Wang	
Subtask 8 **Quantification and statistical analysis.**	4-6 month	Dr. Wang	Dr. Miller
Milestone(s) Achieved 1. A series of myelin-imaging compounds have been synthesized for optimization 2. Systematic structure-activity relationship	1-6 months	Dr. Wang	Dr. Miller

studies have been conducted 3. A lead compound has been identified suitable for PET imaging of myelination			
Local IRB/IACUC Approval	Yes		
ACURO Approval	n/a		
Major Task 2: Preparation and use of *Plp-Akt*-DD transgenic mice for validation of myelin imaging agents through longitudinal optical imaging studies.			
Subtask 1 **Animal preparation (24 animals)**	7-8 months		Dr. Miller
Subtask 2 **Immunohistochemistry**	8-9 months		Dr. Miller
Subtask 3 **Chemical staining**	7-9 months	Dr. Wang	
Subtask 4 **Co-registration of fluorescent and X-ray images**	8-9 months	Dr. Wang	
Subtask 5 **Near-infrared fluorescence *in vivo* imaging**	9-10 months	Dr. Wang	
Subtask 6 **Quantification and statistical analysis**	9-10 months	Dr. Wang	Dr. Wang
Milestone(s) Achieved: 1. An imaging agent termed DBT has been synthesized 2. DBT has been evaluated through systematic tissue staining 3. DBT has been used for longitudinal imaging studies	7-10 months	Dr. Wang	Dr. Miller

Specific Aim 2: Efficacious Evaluation of Selected Therapeutic Agents by MicroPET Imaging			
Major Task 3 **Longitudinal imaging of Demyelination and Remyelination in spinal cord following Mesenchymal Stem Cells (MSC) Treatment**			
Subtask 1 **Preparation of LPC model of focal demyelination in the spinal cord**	10-12 months		Dr. Miller
Subtask 2 **Mesenchymal stem cell (MSC) Treatment**	11-12 Months		Dr. Miller
Subtaks 3 **In vivo PET imaging**	11-12 months	Dr. Wang	
Milestone(s) Achieved: **1. LPC model of focal demyelination in the spinal cord has been successfully prepared.** **2. The mice has been subsequently treated with mesenchymal stem cells (MSC).** **3. PET imaging has been successfully conducted.**	11-12 months	Dr. Wang	Dr. Miller